



The Sima de los Huesos Crania: Analysis of the cranial breakage patterns



Nohemi Sala ^{a, b, c, *}, Ana Pantoja-Pérez ^{c, a, d}, Juan Luis Arsuaga ^{c, d}, Adrián Pablos ^{e, f, a, c}, Ignacio Martínez ^{a, c}

^a Área de Antropología Física, Departamento de Ciencias de la Vida, Universidad de Alcalá, Madrid, Spain

^b Institut für Ur- und Frühgeschichte und Archäologie des Mittelalters Abteilung für Ältere Urgeschichte und Quartärökologie, Eberhard-Karls Universität Tübingen, Schloss Hohentübingen, 72070 Tübingen, Germany

^c Centro Mixto UCM-ISCIII de Evolución y Comportamiento Humanos, Madrid, Spain

^d Departamento de Paleontología, Facultad Ciencias Geológicas, Universidad Complutense de Madrid, Spain

^e Centro Nacional de Investigación sobre Evolución Humana-CENIEH, Burgos, Spain

^f Paleoanthropology, Senckenberg Center for Human Evolution and Paleoenvironment, Eberhard Karls Universität Tübingen, Germany

ARTICLE INFO

Article history:

Received 29 March 2016

Received in revised form

1 June 2016

Accepted 3 June 2016

Keywords:

Taphonomy

Bone breakage

Atapuerca

Interpersonal violence

ABSTRACT

The Sima de los Huesos (SH) site has provided the largest collection of hominin crania in the fossil record, offering an unprecedented opportunity to perform a complete Forensic-Taphonomic study on a population from the Middle Pleistocene. The fractures found in seventeen crania from SH display a postmortem fracturation pattern, which occurred in the dry bone stage and is compatible with collective burial assemblages. Nevertheless, in addition to the postmortem fractures, eight crania also display some typical perimortem traumas. By using CT images we analyzed these fractures in detail. Interpersonal violence as a cause for the perimortem fractures can be confirmed for one of the skulls, Cranium 17 and also probable for Cranium 5 and Cranium 11. For the rest of the crania, although other causes cannot be absolutely ruled out, the violence-related traumas are the most plausible scenario for the perimortem fractures. If this hypothesis is confirmed, we could interpret that interpersonal violence was a recurrent behavior in this population from the Middle Pleistocene.

© 2016 Elsevier Ltd. All rights reserved.

1. Introduction

The main objective of the present work is to describe and to quantify the fracture patterns observed in the Sima de los Huesos – SH– (Atapuerca, Burgos, Spain) hominin crania, to compare them with other fossil hominin crania (both Neandertal and *Homo sapiens*) presumed to be from burials, and with other archaeological samples. Another objective is to discern whether a recently reported case of interpersonal violence in the assemblage (Sala et al., 2015b) is an isolated case or if there are other similar cases in this Middle Pleistocene population.

The distinguishing of fresh bone fractures (antemortem and perimortem) from dry bone fractures (postmortem) allows for an interpretative approach to the cause of death (in forensic sciences),

to the behavior of the populations studied (in anthropology), and to the taphonomic processes involved in the site formation (in archaeological contexts) (Jordana et al., 2013b). The timing of antemortem (i.e. before death) fractures, perimortem trauma (i.e., at or around the time of death), and postmortem modifications (i.e. occurring after death) is discernible (Kimmerle and Baraybar, 2008), especially in cranial remains.

Antemortem injuries are distinguished based on evidence of healing (bone remodeling), such as abnormal bone growth, callus formation, abnormal bone shape, or characteristics associated with an infection (Ortner, 2008). In the fossil record, there are several cases of cranial antemortem (healed) fractures such as: Middle Pleistocene remains of Maba 1 (Wu et al., 2011), Atapuerca-Trinchera Galería parietal (Arsuaga et al., 1999), as well as at least eight of the Atapuerca-SH crania (Gracia-Téllez et al., 2013; Pérez et al., 1997) and Late Pleistocene hominins such as Dolní Věstonice 3, 11/12, 13, 15 and 16 (Trinkaus and Svoboda, 2006), Feldhofer 1 (Schultz, 2006), Krapina 4, 20, 31, 34.7 (Gardner and Smith, 2006; Radovčić et al., 1988), Qafzeh 11 (Coqueugniot et al.,

* Corresponding author. Área de Antropología Física, Departamento de Ciencias de la Vida, Universidad de Alcalá, Madrid, Spain.

E-mail address: nohemisala@rocketmail.com (N. Sala).

2014), Saint Césaire 1 (Zollikofer et al., 2002), Šal'a 1 (Sládek et al., 2002), Shanidar 1 and 5 (Berger and Trinkaus, 1995; Trinkaus, 1983), Sunghir 5 (Trinkaus et al., 2014), Xujiayao 5a, 8 and 12 (Wu and Trinkaus, 2015) among others.

Perimortem fractures, in contrast to antemortem injuries, exhibit no evidence of healing. Furthermore, perimortem fractures, unlike postmortem fractures, occur while the bone is still fresh (i.e., surrounded by soft tissue and/or preserving the organic matrix) (Ortner, 2008; Ubelaker and Adams, 1995). Injuries occurring at the time of death may be classified as perimortem, but they can also occur after death, while the body still preserves soft tissue. Following forensic criteria (Martin and Harrod, 2015), the discovery and analysis of perimortem fractures can help to identify the cause of death (accidental, such as free-falls or violence-related) or whether the processes happened shortly after death. Nevertheless, the application of these criteria to the fossil record, where soft tissues are not preserved, is more limited than in current cases. In the Pleistocene fossil record, there is some evidence of cranial and postcranial perimortem fractures, but there are only few examples that are tentatively considered cases of interpersonal violence, among which is one of the Sima de los Huesos individuals (Cr-17) (Sala et al., 2015b). The fact that we have isolated cases documenting violence in the fossil record makes it difficult to interpret whether this behavior was habitual or rare during the Pleistocene.

Finally, the postmortem cranial fractures occur on defleshed bones that contain no muscles or skin, and the process undoubtedly occurs after the individual's death. At this stage, the fracturing characteristics are easily recognized because the bones behave as a rigid body; i.e., fresh bone has more energy when it absorbs stress than a dry bone (Evans, 1957; Gurdjian and Lissner, 1945). In the archaeological and paleontological records, the analysis of postmortem fractures is relevant since it may provide taphonomic information about the site formation and post-depositional processes (Dirks et al., 2015; Sala et al., 2015a). In addition, it is crucial to recognize this state of bone breakage from the others that have behavioral implications.

There are taphonomic studies on anthropic modification in contexts of cannibalism, e.g., Gran Dolina TD-6 (Atapuerca, Spain) hominin remains (Saladié et al., 2011, 2012), Moula-Guercy (France) (Defleur et al., 1999), Gough's cave (Somerset, UK) (Bello et al., 2011, 2015), El Mirador (Atapuerca, Spain) (Cáceres et al., 2007), Herxheim (Germany) (Boulestin and Coupey, 2015), and others (Boulestin, 2012). There are also some papers regarding carnivore activity on fossil crania (Arsuaga et al., 2007; Boaz et al., 2004; Sala et al., 2014). In archaeological contexts there are studies of fracture patterns on cranial remains (Berryman and Haun, 1996; Jordana et al., 2009; Kanz and Grossschmidt, 2006; Messina et al., 2013; Mirazón-Lahr et al., 2016; Spencer, 2012; Walker, 1989); nevertheless, there is a lack of specific research addressing fracturation analyses of hominin cranial in particular and flat bones in general in Pleistocene contexts.

2. Material and methods

2.1. Sima de los Huesos site

The Sima de los Huesos is a small karstic chamber at the foot of a shaft located deep inside an underground karst system (Arsuaga et al., 1997). Inside this chamber, twelve Lithostratigraphic Units (LU) were defined, but only one of them (LU-6) contains hominin remains (Fig. 1) (Aranburu et al., 2016). LU-6 consists of plastic red clays with a high density of hominin and carnivore fossils (mainly the bear *Ursus deningeri*). To date, ~6800 human fossil fragments, belonging to at least 28 individuals, are represented in this stratigraphic level (LU-6) (Arsuaga et al., 2014; Bermúdez de Castro et al.,

2004). Using a variety of techniques, the hominin-bearing layer could be assigned to a period around 430 ka (Arsuaga et al., 2014). A small portion (<7% of the current collection) of the hominin fossils from LU-6 was moved from the "in situ" levels to the uppermost part of the site and disturbed and trampled by non-professional diggers before the formal excavation period (Arsuaga et al., 1997).

During the time in which the hominin bones accumulated at the SH site, the only possible access routes to the site were through deep (c.13 m) vertical chimneys (Aranburu et al., 2016). Given the skeletal part representation in the collection, composed of all anatomical parts (Arsuaga et al., 1997, 2015), it is likely that entire corpses were deposited at the site. There are no cutmarks on any of the 6800+ hominin bones and no single ungulate fossil has been recovered to date.

The site formation origin, especially the causes for the hominin accumulation, has been highly debated, with different possible hypotheses proposed (Aguirre, 2000; Andrews and Fernández-Jalvo, 1997; Arsuaga et al., 1990, 1997; Arsuaga and Martínez, 2004; Bocquet-Appel and Arsuaga, 1999; Díez, 1990). Some of these possible scenarios of site formation were recently rejected. Firstly, the proposal that carnivores were accumulators of the hominin bones was discarded, since tooth marks are rare in the hominin collection (Sala et al., 2014). Actually, tooth marks on cranial remains were found in 1.10% (four fragments) of the cranial sample, including score marks on Cr-3 and Cr-4 (Sala et al., 2014). On the other hand, the sedimentological features of the hominin-bearing unit argue against the hypothesis that the hominin bones were transported to SH from a locus of primary accumulation far from their present day location (Aranburu et al., 2016). Lastly, accidental causes for all hominin arrivals to the SH chamber were also recently ruled out, at least for the individual represented by Cr-17, because this individual was already dead before its arrival at the site (Sala et al., 2015b). On the other hand, the pattern of postcranial fractures in the assemblage indicates that a large majority occurred after burial and resulted from the overlying sediment pressure, which is compatible with collective burial assemblages (Sala et al., 2015a). Nevertheless, a small proportion (~4%) of postcranial perimortem fractures were also found (Sala et al., 2015a), indicating that a specific study of cranial fractures was necessary, since the physical and morphological features of cranial remains allow for more accurate interpretations of the timing and causes of perimortem fractures.

2.2. The SH cranial sample

The cranial sample from SH is a large collection composed of >1850 bone fragments. Of these, >560 cranial fragments have been fitted together to form 17 specimens that represent the same number of individuals (Fig. 2). These 17 individuals show different ages-at-death (Table 1): five immature, three late adolescent, and nine fully adults (Arsuaga et al., 2014). In this work we include the analysis of all the fragments that form the 17 cranial individuals.

2.3. Comparative sample

In addition to the SH sample, in this work Neandertal adult specimens (La Ferrassie 1, La Chapelle-aux-Saints 1 and La Quina H5) and Upper Paleolithic *H. sapiens* individuals (Cro-Magnon 1–3 and Abri Pataud) are included, all of which are interpreted as burials (Defleur, 1993; Henry-Gambier, 2002; Maureille and Peer, 1998; Rendu et al., 2014). Furthermore, we compared our results with bibliographic resources of osteological sites that are considered standards of fresh bone fractures in the literature (Agris Mesolithic site and Châteliers du Vieil-Auzay, France, from the Neolithic period) and dry bone fractures (Corconne Neolithic

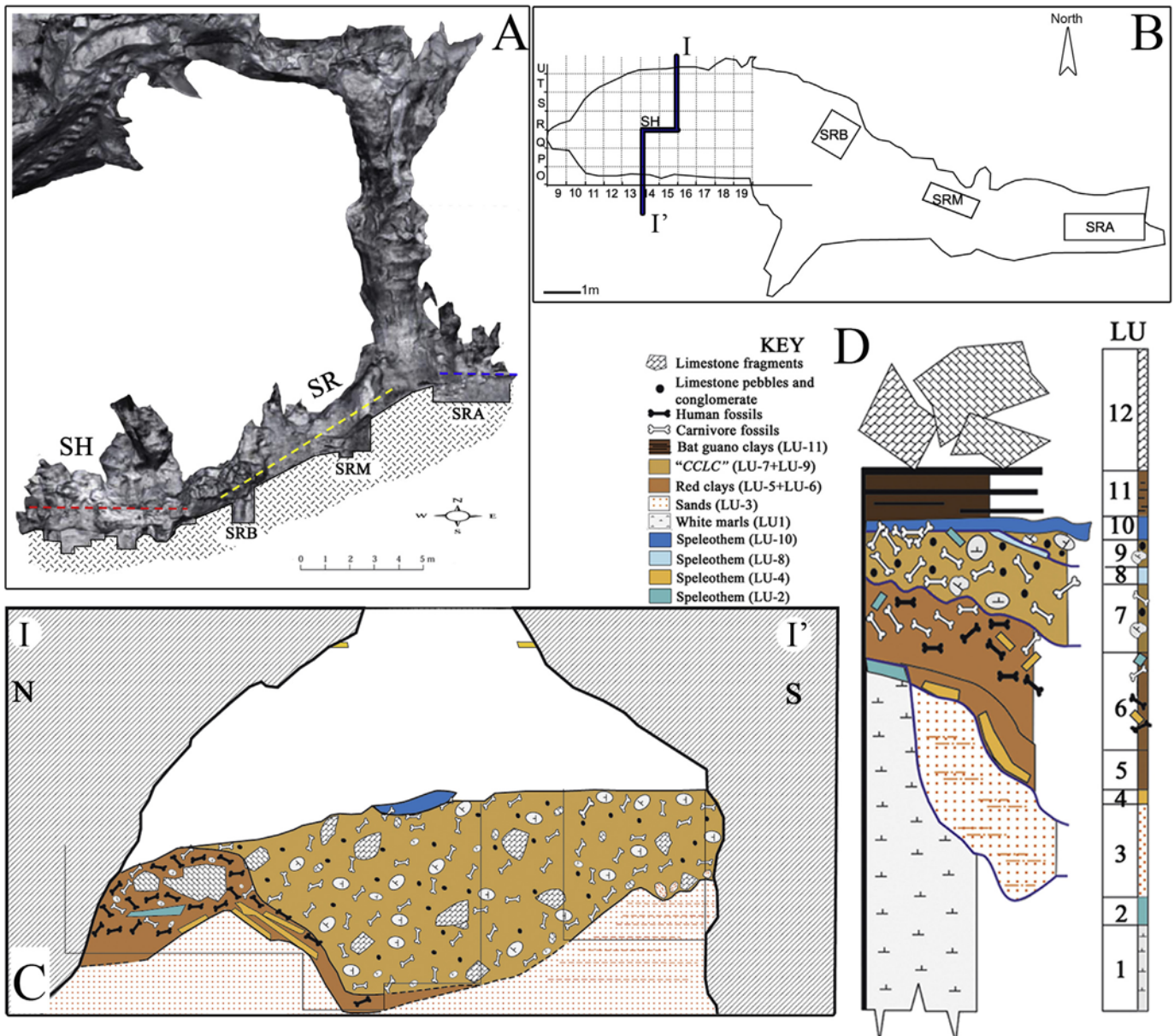


Fig. 1. A) 3D scan of the Sima de los Huesos chamber showing the different parts of the SH site: SH = Sima de los Huesos proper; SR = Sima Ramp; SRB = Sima Rampa Baja = SRA: Sima Rampa Media and SRA = Sima Rampa Alta. B) Overview layout of SH with the cross-section I–I' represented. C) North-South cross section (I–I') showing the hominin bearing layer (LU-6) attached to the North wall of the site. D) Composite stratigraphic section of the SH site with all the Lithostratigraphic Units (LU) in stratigraphical position. The colors used in C and D correspond to those of the Munsell color system for wet sediment. Modified from Arsuaga et al. (2014) and Aranburu et al. (2016).

material and Villedubert Chalcolithic, France, sites) (Jordana et al., 2013b).

2.4. Methodological procedure

In order to examine the taphonomic aspects of the cranial collection, detailed visual inspection directly on the bone remains, as well as virtual three-dimensional images were used. Observations were made with a Nikon SMZ800 Stereoscopic light microscope. Detailed images of the fractures were made with a Nikon Digital Sight DS-Fi1 camera.

3D imaging provides an opportunity to analyze critical aspects of the fracture properties (Fleming-Farrell et al., 2013), especially when the different cranial fragments are glued together. The SH

crania were CT scanned in the coronal plane using an industrial YXLON MU 2000- CT scanner at the Universidad de Burgos (Spain) (See Supplementary Information Table 1 for CT parameters). CT images were used to assess cranial fractures and accurately assess fracture timing. Virtual (3D CT) models of each cranium were generated from the resulting slices using the Mimics 16.0 (Materialise N.V.) software package.

In order to determine the timing (perimortem vs. postmortem) of cranial bone fracturing and the possible causes of perimortem injuries (accidental vs. intentional) of skull bone fracture of the SH sample, we studied the following parameters: fracture type, fracture location, fracture trajectory, fracture angle, presence/absence of cortical delamination, and edge texture (Fig. 3, Table 2). Some cranial fragments, especially those recovered in the disturbed

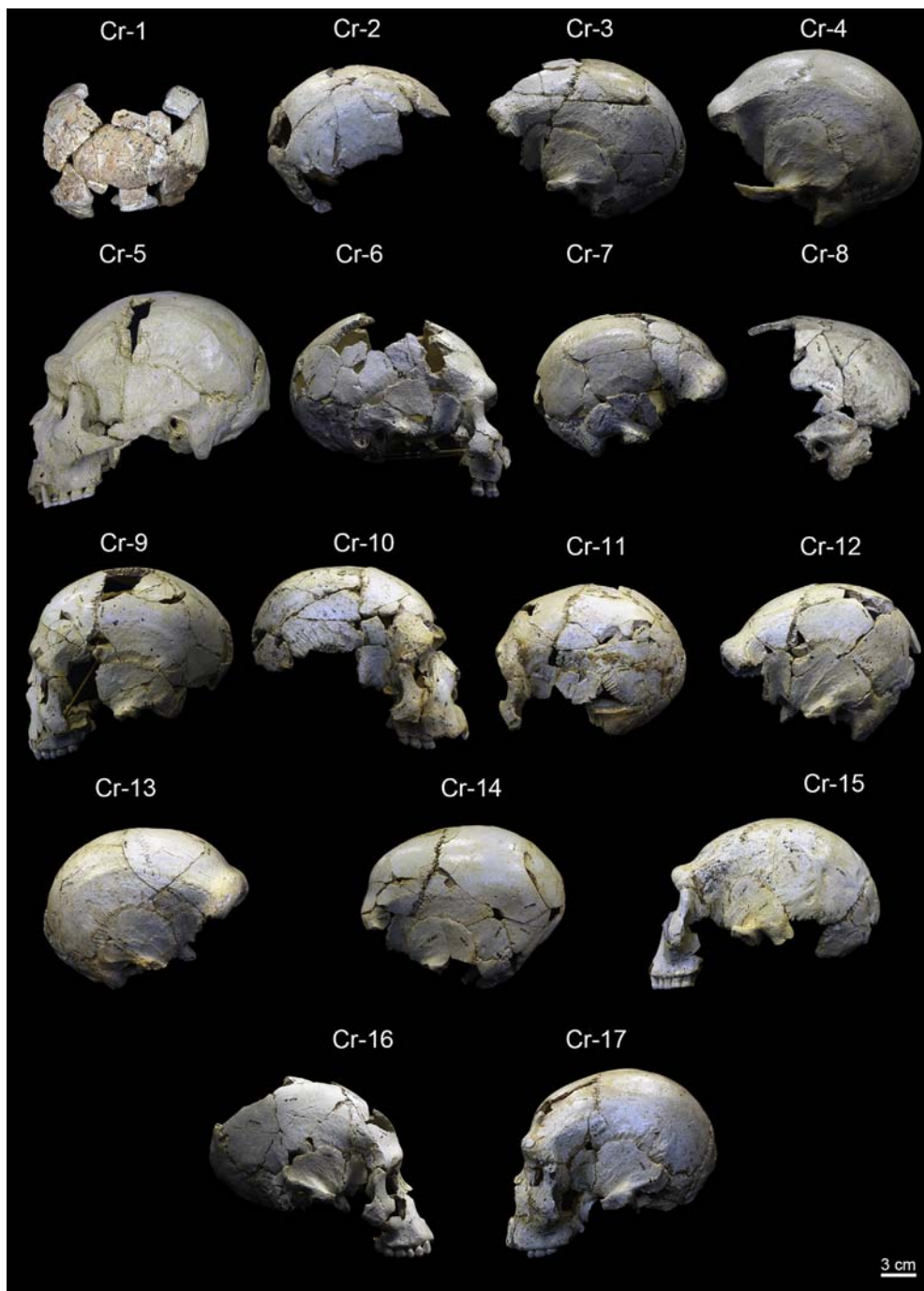


Fig. 2. Seventeen Middle Pleistocene crania from the Sima de los Huesos site. All specimens are shown in lateral view, except the Cr-1 shown in posterior view.

sediment (trampled by cavers), display recent fractures that are easily recognizable due to the different coloration of the fracture plane. These fractures were excluded from the fracture analysis. For the fracturation analysis, we focus on the cranial vault bones. Cranial vault bones consist of the frontal, parietal, temporal, sphenoid, and occipital bones. Of these, the parietal, occipital and frontal bones are characterized by outer and inner tables of dense cortical bone separated by a trabecular diploë. This structural pattern makes these vault bones more diagnostic than the thinner cranial bones (e.g., those of the face) in order to interpret the breaking patterns. Therefore, in this work, we focus on these cranial vault fractures.

2.4.1. Fracture outline

The general morphology of the fractures can be straight, curved, circular, concentric, radial, and a combination of circular and radial. Fracture morphology is not a reliable indicator of bone state at the time of fracture (Jordana et al., 2013b). Nevertheless, this parameter can be useful in describing the perimortem traumas because the fracture outline depends on many factors: velocity of the impact, impacting object (blunt vs. sharp traumas), or force (Gurdjian and Lissner, 1945; Lovell, 1997). In this paper, the classification of cranial vault fractures proposed by Galloway and Wedel (2014) is used as follows: *Linear fractures* (Fig. 3A) include any single fracture that passes through the outer and/or inner tables. *Depressed fractures*

Table 1

Cranial inventory of the SH site.

Specimen	Age at death ^a	Description ^a	Number of fragments
Cranium 1	Adult	Partial calvarium	14
Cranium 2	Adult	Partial calvarium	27
Cranium 3	Immature	Almost complete calvarium	34
Cranium 4	Adult	Complete calvarium	2
Cranium 5	Adult	Complete skull	14
Cranium 6	Immature	Almost complete cranium	44
Cranium 7	Late adolescent	Almost complete calvarium	52
Cranium 8	Adult	Partial calvarium	18
Cranium 9	Immature	Almost complete skull	57
Cranium 10	Late adolescent	Partial cranium	25
Cranium 11	Immature	Partial cranium	53
Cranium 12	Adult	Almost complete calvarium	32
Cranium 13	Adult	Almost complete calvarium	42
Cranium 14	Immature	Almost complete calvarium	27
Cranium 15	Adult	Partial skull	32
Cranium 16	Late adolescent	Partial cranium	40
Cranium 17	Adult	Almost complete cranium	52

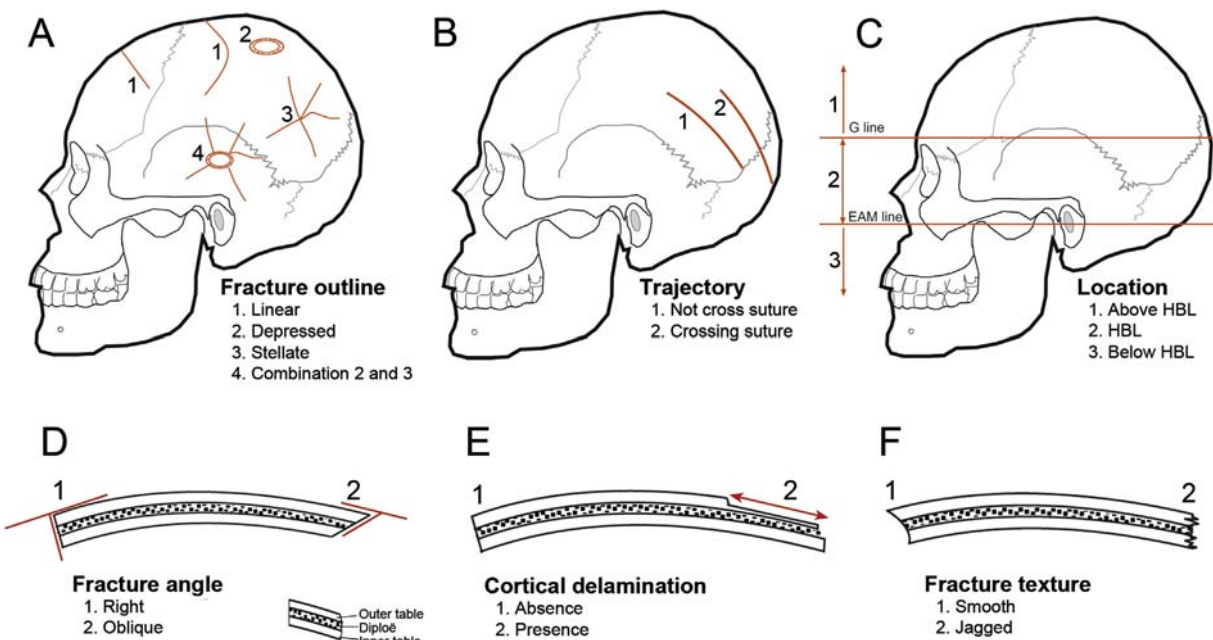
^a Data from Arsuaga et al. (2014).

Fig. 3. Variables studied in the cranial remains from Sima de los Huesos. The figure represents the fracture properties: fracture outline (following the classification proposed by Galloway and Wedel (2014), trajectory, location regarding the “Hat Brim Line” sensu Kremer et al. (2008), fracture angle, cortical delamination and fracture texture (Jordana et al., 2013b) analyzed in this work.

Table 2

Perimortem (fresh bone) vs postmortem (dry bone) fracture properties.

Feature	Description	Perimortem	Postmortem	Literature
Fracture texture	Morphology of the broken bone surface	Smooth	Jagged	1
Fracture angle	Angle between the cortical table and surface of the fracture	Oblique	Right	2
Cortical delamination	Cleavage between the diploë and the inner/outer table	Present	Absent	3
Fracture trajectory	Fractures cross through unfused sutures	Fractures can cross unfused sutures	Fractures are interrupted in unfused sutures	4

1: Fleming-Farrell et al., 2013; Johnson 1985; Jordana et al., 2013a; Ortner 2008; Outram et al., 2005; Villa and Mahieu 1991; Wieberg and Wescott 2008.

2: Fleming-Farrell et al., 2013; Johnson 1985; Jordana et al., 2013a,b; Ortner 2008; Outram et al., 2005; Villa and Mahieu 1991; Wheatley 2008; Wieberg and Wescott 2008.

3: Berryman and Haun 1996; Jordana et al., 2013a.

4: Evans 1957; Fleming-Farrell et al., 2013; Gurdjian and Lissner 1945; Jordana et al., 2013b.

Table 3

Fracture properties of the Sima de los Huesos crania.

Specimen N	Fracture outline					Angle ^a		Surface		Trajectory		Cortical delamination ^b		
	Linear-straight	Linear-curved	Depressed	Stellate	Depressed+stellate	Right	Oblique	Smooth	Jagged	NCS	CS	Presence	Absence	
CR-1	13	13 (100%)	0	0	0			13 (100%)	0	0	13 (100%)	0	0	13 (100%)
CR-2	30	27 (90%)	3 (10.8%)	0	0			27 (90%)	3 (10%)	0	30 (100%)	30 (100%)	0	30 (100%)
CR-3	37	31 (83.8%)	4 (10.8%)	0	0	2 (5.4%)		34 (91.9%)	3 (8.1%)	3 (8.1%)	34 (91.9%)	35 (94.6%)	2 (5.4%)	4 (10.8%)
CR-4	0	0	0	0	0			0	0	0	0	0	0	0
CR-5	5	4 (80%)	0	1 (20%)	0	0		4 (80%)	1 (20%)	1 (20%)	4 (80%)	5 (100%)	0	1 (20%)
CR-6	36	35 (97.2%)	1 (2.8%)	0	0	0		32 (88.9%)	4 (11.1%)	0	36 (100%)	36 (100%)	0	36 (100%)
CR-7	57	45 (78.9%)	10 (17.5%)	1 (1.8%)	1 (1.8%)			50 (87.7%)	7 (12.3%)	4 (7%)	53 (93%)	56 (98.2%)	1 (1.8%)	2 (3.5%)
CR-8	15	15 (100%)	0	0	0			15 (100%)	0	0	15 (100%)	15 (100%)	0	15 (100%)
CR-9	45	33 (73.3%)	11 (24.4%)	0	0	1 (2.2%)		40 (88.8%)	5 (11.1%)	1 (2.2%)	44 (97.8%)	41 (91.1%)	4 (8.9%)	2 (4.4%)
CR-10	28	26 (92.9%)	2 (7.1%)	0	0	0		27 (96.4%)	1 (3.6%)	1 (3.6%)	27 (96.4%)	28 (100%)	0	1 (3.6%)
CR-11	56	49 (87.5%)	6 (10.7%)	1 (1.8%)	0	0		54 (96.4%)	2 (3.6%)	4 (7.1%)	52 (92.9%)	53 (94.6%)	3 (5.4%)	53 (94.6%)
CR-12	37	27 (73%)	10 (27%)	0	0	0		33 (89.2%)	4 (10.8%)	4 (10.8%)	33 (89.2%)	31 (83.8%)	6 (16.2%)	5 (13.5%)
CR-13	33	22 (66.7%)	9 (27.3%)	1 (3%)	0	1 (3%)		30 (90.9%)	3 (9.1%)	3 (9.1%)	30 (90.9%)	33 (100%)	0	5 (15.2%)
CR-14	38	34 (89.5%)	1 (2.6%)	0	2 (5.3%)	1 (2.6%)		35 (92.1%)	3 (7.9%)	3 (7.9%)	35 (92.1%)	38 (100%)	0	3 (7.9%)
CR-15	35	34 (97.1%)	1 (2.9%)	0	0	0		35 (100%)	0	0	35 (100%)	35 (100%)	0	0
CR-16	26	25 (96.2%)	1 (3.82%)	0	0	0		26 (100%)	0	0	26 (100%)	26 (100%)	0	0
CR-17	25	18 (72%)	5 (20%)	2 (8%)	0	0		23 (92%)	2 (8%)	2 (8%)	23 (92%)	25 (100%)	0	2 (8%)
TOTAL	516	438 (84.9%)	64 (12.4%)	6 (1.2%)	3 (0.6%)	5 (1%)		478 (92.6%)	38 (7.4%)	26 (5%)	490 (95.0%)	500 (96.9%)	16 (3.1%)	28 (5.4%)
														488 (94.6%)

N = Number of fractures analyzed. NCS: Not crossing suture. CS: Crossing suture.

^a See Fig. 4.^b See Table 4.

result from a concentration of energy sufficient to cause local failure to the bone and may be characterized as penetrating fractures with or without associated radial fractures (Fig. 3A). *Stellate fractures* of the vault consist of multiple radiating linear fractures that originate at the point of impact where the tensile forces become most pronounced. Stellate fractures can be associated with depressed fractures at the point of impact (Fig. 3A).

2.4.2. Fracture trajectory (Fig. 3B)

The behavior of the fracture in terms of trajectory is variable in cranial remains, depending on the soft tissue content. A relatively thin layer of soft tissue (i.e., the scalp) allows the propagation of the strain across the sutures (Evans, 1957). In the dry skull (without soft tissue), the propagation of the strain tends to be interrupted by the suture line, which acts as a barrier to propagation (Evans, 1957; Fleming-Farrell et al., 2013; Gurdjian and Lissner, 1945; Jordana et al., 2013a), especially when the sutures are unfused (i.e., in immature individuals). For this reason we observed whether the fracture crosses through sutures (typical of the perimortem stage) or, on the contrary, whether the fractures are interrupted by the sutures (postmortem breakage) (Table 2).

2.4.3. Fracture location

For the perimortem cranial fractures, the location of the traumatic lesion is relevant, since it can help us to discriminate accidental falls from intentional blunt head injuries. For the analysis of the lesion location, we consider: i) the bone affected (frontal, parietal, etc.); ii) the side of the lesion (right or left), and iii) the location with respect to the “hat brim line” (HBL). HBL (Fig. 3C) was defined as the area located between two lines parallel to a line inspired by the Frankfort horizontal plane (horizontal plane passing through right and left portion points and the left orbitale), the

superior margin passing through the glabella (G line) and the inferior margin passing through the center of the external auditory meatus (EAM line) (Guyomarc'h et al., 2010; Kremer et al., 2008; Kremer and Sauvageau, 2009). According to the HBL rule, an injury located at the level where the brim of a hat would lie is more likely the result of a fall, while a blow would generally produce a wound above this line (Guyomarc'h et al., 2010).

2.4.4. Fracture angle

This is the angle formed by the fracture surface and the bone cortical table (Fig. 3). This angle is mostly acute or obtuse in fresh bones but occurs at ~90° in dry bones (Table 2) on the long bones (Sala et al., 2015a; Villa and Mahieu, 1991; Wheatley, 2008; Wieberg and Wescott, 2008) and the skull (Fleming-Farrell et al., 2013; Jordana et al., 2013b; Lovell, 1997; Quatrehomme and Iscan, 1997). Fracture angle was measured on the CT 3D virtual reconstructions using Mimics 16.0 (Materialise N.V.) software tools. We consider right angles those that are between 70° and 110°.

2.4.5. Cortical delamination

Cortical delamination (Fig. 3E) or bevelling is the cleavage between the diploe and the inner/outer table (Berryman and Haun, 1996; Jordana et al., 2013b). Large cortical delamination (greater than 10.5 mm) only occurs on green bone fracturing (Jordana et al., 2013b) (Table 2). The maximum width of delamination was measured with an electronic calliper directly on the bone and on the CT reconstructions using Mimics 16.0 (Materialise N.V.) software tools.

2.4.6. Fracture texture

Texture refers to the structure and thus to the disposition of collagen fibres exposed by the fracture line (Jordana et al., 2013b;

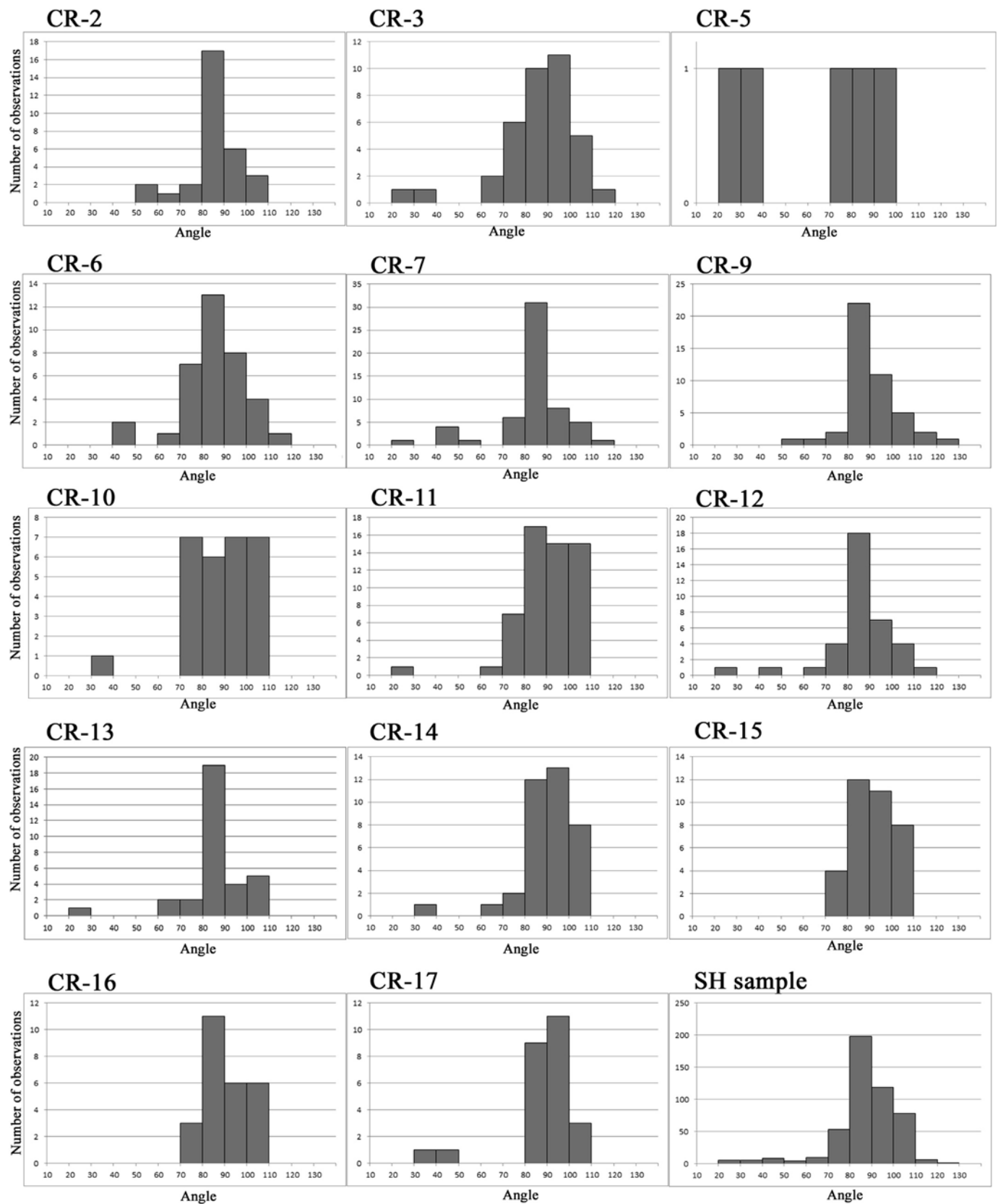


Fig. 4. Histograms in which the fracture angles are represented in the cranial individuals from the Sima de los Huesos assemblage.

Table 4
Cortical delamination measurements.

	N	Mean	Maximum	Std. Dev.
CR-3	5	6.18	7.84	1.26
CR-5	2	10.26	11.79	2.17
CR-7	3	6.45	6.94	0.79
CR-9	3	6.21	8.30	2.43
CR-10	1	9.95	—	—
CR-11	7	8.87	15.63	4.35
CR-12	9	7.72	14.34	4.08
CR-13	6	7.44	16.67	4.69
CR-14	3	5.26	5.84	0.99
CR-17	8	9.23	13.53	2.96

N: Number of measurements taken in different points and different cross sections or slices of the fractures.

Std. Dev: Standard Deviation.

Villa and Mahieu, 1991). Two attributes are taken into consideration: smooth or jagged (Fig. 3F). Although this parameter has been questioned by some authors (Johnson, 1985; Villa and Mahieu, 1991), the texture can be used to study the timing of bone fracturing (Table 2) since the broken bone surfaces tend to be smooth in fresh bone with a regular collagen fibre structure but jagged in dry bones (Jordana et al., 2013b,a).

In order to compare the fracture properties of all SH cranial specimens with other comparative samples, we performed a Multiple Correspondence Analysis (MCA) using the STATISTICA 8.0 (StatSoft, 2007) software.

3. Results

The analysis of cranial fractures shows that all specimens, except the Cr-4, display vault fractures (94.1% of the SH collection). None of the individuals display taphonomic cranial deformation. A total of 516 fracture planes were examined in terms of fracture outline, fracture angle, texture surface, trajectory and cortical delamination (Table 3).

Regarding the fracture outline, 84.9% of the total sample display straight morphology, followed by curved outline (12.4%). Depressed, stellate, and a combination of the two are present in Cr-3, Cr-5, Cr-7, Cr-9, Cr-11, Cr-13, Cr-14 and Cr-17 (2.6% of the total sample).

With respect to the fracture angle between the internal and external bone tables, 92.6% of the total sample display right angles. Fig. 4 represents the distribution of angles by cranial specimen with 10-degree intervals. As is represented in the figure, most angles lie between 70° and 110°. Nevertheless, some crania also display

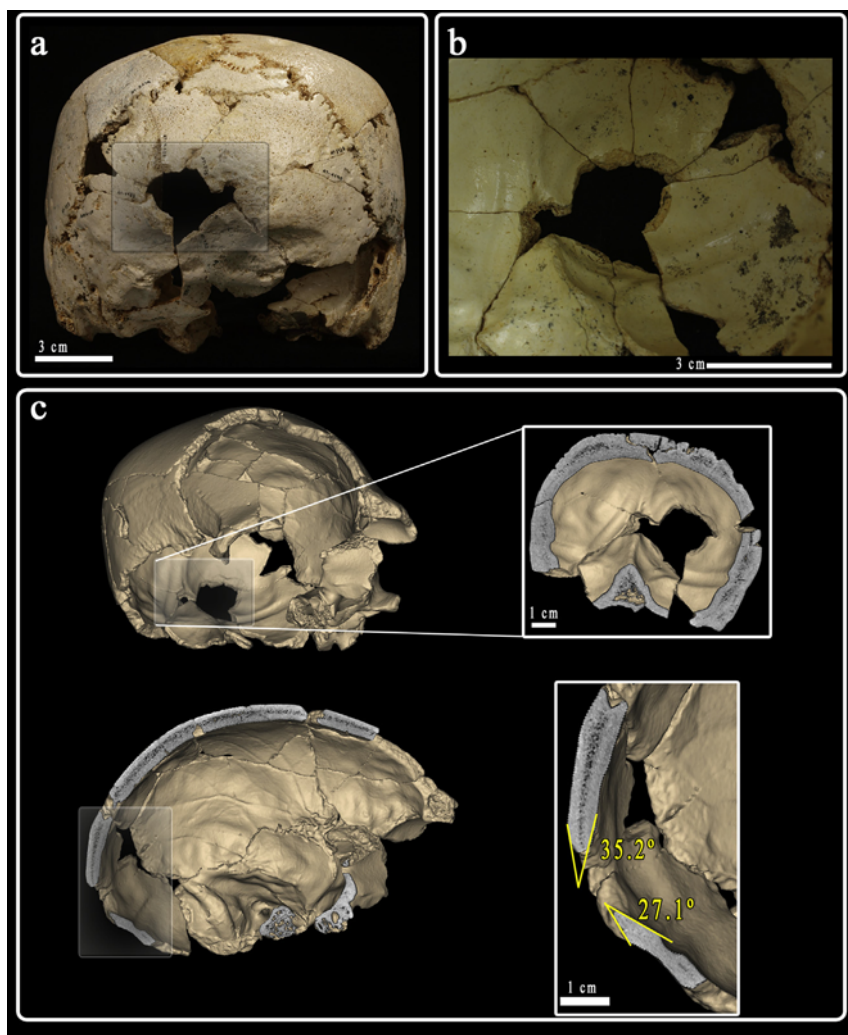


Fig. 5. Cranium 3 (Cr-3) perimortem fractures on occipital bone. a) Posterior view; b) Detailed endocranial view of the traumatic fractures; c) CT analysis of the Cranium 3 traumas and detail of the cross-sections showing the acute angles (35.2° and 27.1°) associated with the traumatic fractures.

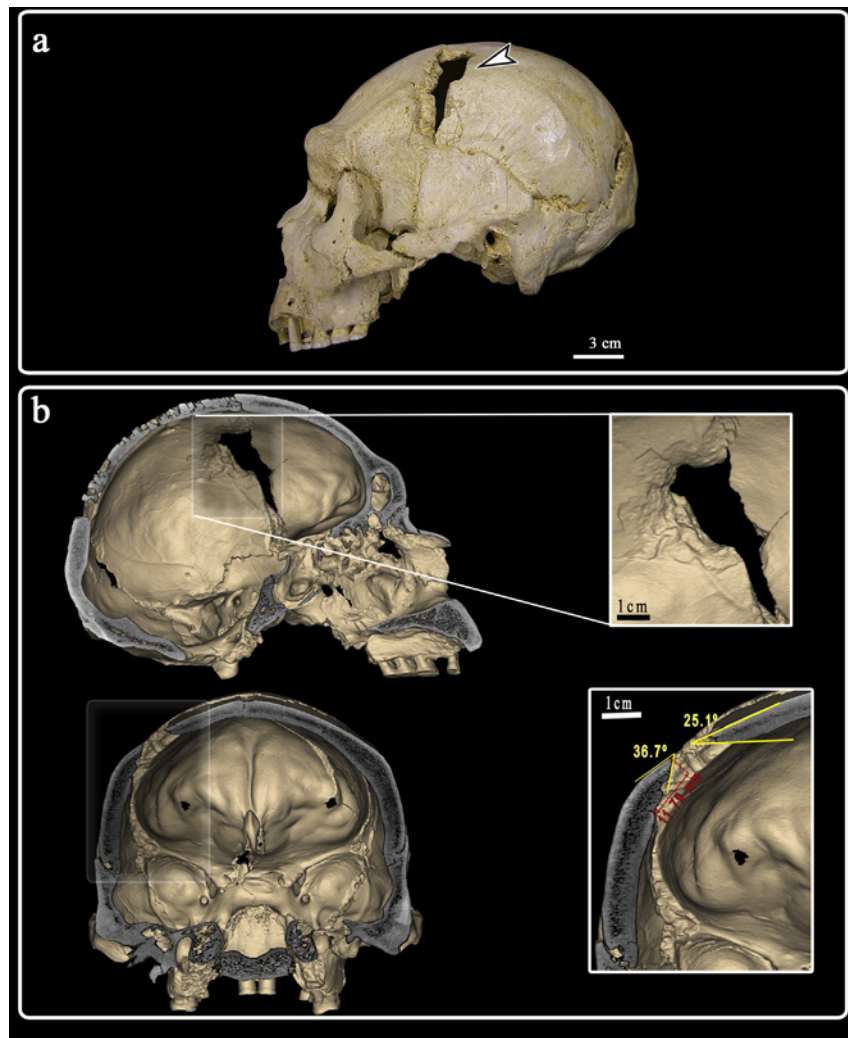


Fig. 6. Cranium 5 (Cr-5) perimortem fracture on the left parietal bone. a) Lateral view of the cranium with the fracture marked by the white arrow; b) CT analysis of the Cranium 5 fracture with a sagittal cross-section where the large cortical delamination is observable in endocranial view and coronal cross-section of the fracture in detail showing the acute fracture angles (36.7° and 25.1°) and the large cortical delamination of the inner table (11.79 mm).

obtuse or acute angles.

Regarding the surface texture of the broken edges, 95% of the analyzed fractures display jagged surfaces (Table 3). Smooth surfaces (5% of the total sample) are present on Cr-3, Cr-5, Cr-7, Cr-9, Cr-10, Cr-11, Cr-12, Cr-13, Cr-14 and Cr-17. On the other hand, 96.9% of the fractures are interrupted by cranial sutures. We only documented fractures crossing sutures in 3.1% of the fractures analyzed, in the Cr-3, Cr-7, Cr-9, Cr-11 and Cr-12. Concerning the cortical delamination, we observed that 5.4% of the fractures display this characteristic associated with fractures. Table 4 shows the metrical data of the maximum cortical delamination measured on the fractures. Large cortical delamination (greater than 10.5 mm) has been documented in Cr-5, Cr-11, Cr-12, Cr-13 and Cr-17.

As previously explained, the fracturing features of the SH skulls are mostly characterized by straight and curved outlines, right angles, jagged surfaces, fractures interrupted by sutures and an absence of cortical delamination features. Actually, those features are the only ones present in some specimens (Cr-1, Cr-2, Cr-8, Cr-15 and Cr-16). Nevertheless, other specimens also display features that differ from the general pattern in some regions and are explained above.

In the occipital bone of the Cr-3 (within the HBL zone) (Fig. 5),

we can observe two connected penetrating depressed fractures with oblique angles (35.2° and 27.1°), smooth surfaces, cortical delamination and radial fractures that cross unfused lambdoid sutures. The diameter of the largest depressed fracture is 20.91 mm.

Cr-5 shows fractures only on the frontal and left parietal bones. The frontal bone fractures follow the general pattern (straight outlines, right angles, jagged surfaces, fractures interrupted by sutures and the absence of cortical delamination). Nevertheless, on the left parietal, above the HBL zone, there is a depressed fracture with oblique angles (25.1° and 36.7°), a smooth surface and the presence of cortical delamination (11.79 mm). All these features are associated with each other (Fig. 6).

Cr-6 displays fractures on frontal, occipital, and parietal bones with a dominance of straight outlines, right angles, jagged surfaces, an absence of cortical delamination and fractures interrupted by sutures. Although some of the fracture angles are oblique (48.82° , 46.04° , 32.74° and 118.4° respectively), these fracture planes are not associated.

In addition to the general pattern fractures, the occipital bone of Cr-7 also displays (below the HBL) a depressed fracture (8.32 mm in diameter) with cortical delamination, oblique angles, smooth surfaces and radial fractures crossing the lambdatic suture (Fig. 7).

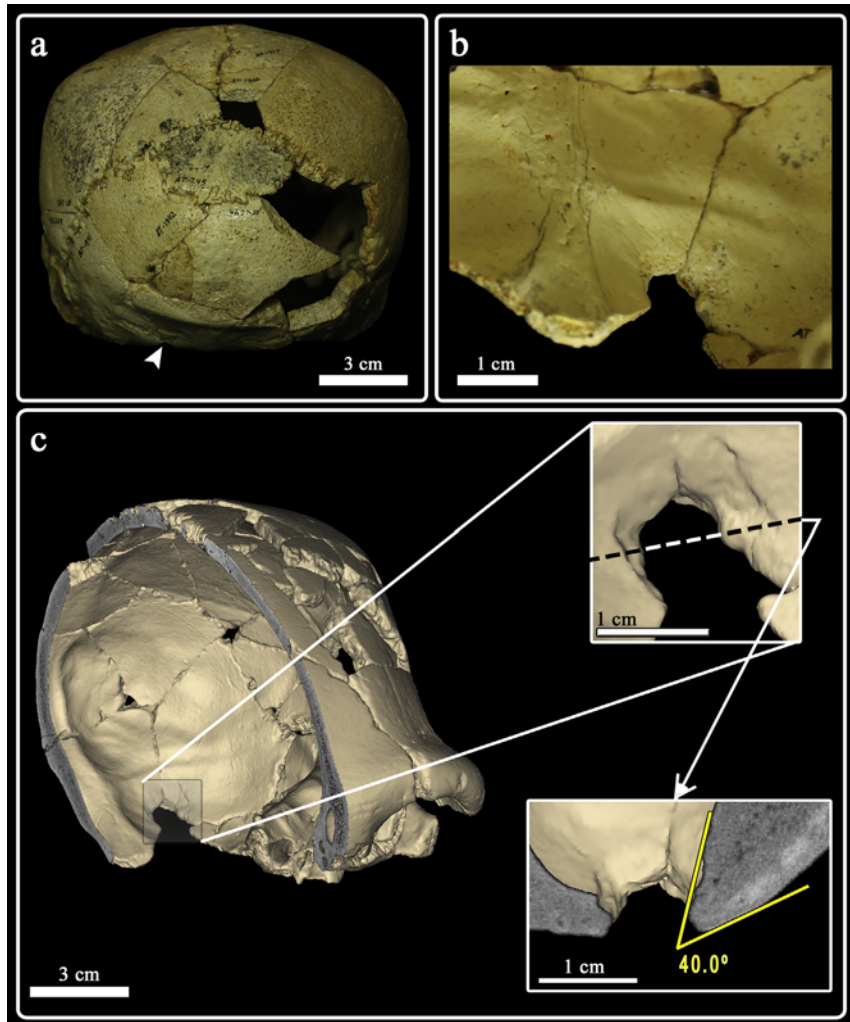


Fig. 7. Cranium 7 (Cr-7) perimortem fracture on the occipital bone. a) Posterior view of Cr-7 with the location of the fracture marked with the white arrow; b) Endocranial view of the perimortem fracture; c) Sagittal cross-section of the Cr-7 virtual CT and detailed pictures showing the cortical delamination in endocranial view and the acute fracture angles (40.0°).

Cr-9 displays a large number of fractures on the cranial vault bones, which are characterized by straight and curved outlines, right angles, jagged surfaces, fractures interrupted by sutures and an absence of cortical delamination features. However, this specimen also has some cases of oblique angles on occipital and frontal bones, one case of cortical delamination on an occipital fracture and four fractures that apparently pass through lambdatic, sagittal and coronal sutures. In this specimen the presence of one depressed fracture on the left side of the occipital bone, below the HBL, is remarkable. This depressed fracture (larger diameter of 13.62 mm) displays oblique angles, the presence of cortical delamination (6.78 mm), as well as a smooth surface (Fig. 8).

Almost all of the Cr-10 fractures are characterized by the general pattern except by one of them observable on the left parietal (within the HBL). In this latter case, cortical delamination is visible, together with an oblique angle (33.41°). Cr-11 displays on the left parietal, above the HBL, a circular-shaped fracture with a diameter of 20.14 mm, characterized by an oblique angle (26.6°) and a smooth surface (Fig. 9).

In the case of Cr-12, some features that are different from the general pattern are observable. In the left and right parietal there are fragments with oblique angles (27.35° , 41.03° and 62.72°), cortical delamination (4.17 mm, 6.25 mm, 14.11 mm and 8.51 mm)

and six fractures crossing cranial sutures (four of them crossing the coronal suture and two crossing the sagittal suture). Nevertheless, these features are not related to each other.

In addition to the general pattern, the right parietal of Cr-13 shows one fracture plane with a smooth surface and the presence of cortical delamination. Furthermore, the presence of one depressed fracture on the left side of the occipital bone within the HBL is notable. This depressed fracture displays oblique angles (28.2°), the presence of cortical delamination, as well as a smooth surface (Fig. 10).

Cr-14 displays two stellate fractures on the left side of the cranium, specifically on the left side of the frontal squama (above the HBL) and the left parietal (within the HBL). In addition, a depressed fracture is observable on the left portion of the occipital bone, close to the asterion. These fractures are characterized by oblique angles, smooth surfaces, and the presence of cortical delamination (Fig. 11).

The bone fragments that comprise the Cr-17 vault show a clear dominance of straight/curved fracture outlines, right angles between the cortical table and the surface of the fracture, jagged surfaces, and an absence of cortical delamination along the fracture edges. Nevertheless, on the left side of the frontal squama, this individual shows two sub-rectangular-shaped fractures, above the HBL, characterized by oblique angles, smooth surfaces, and the

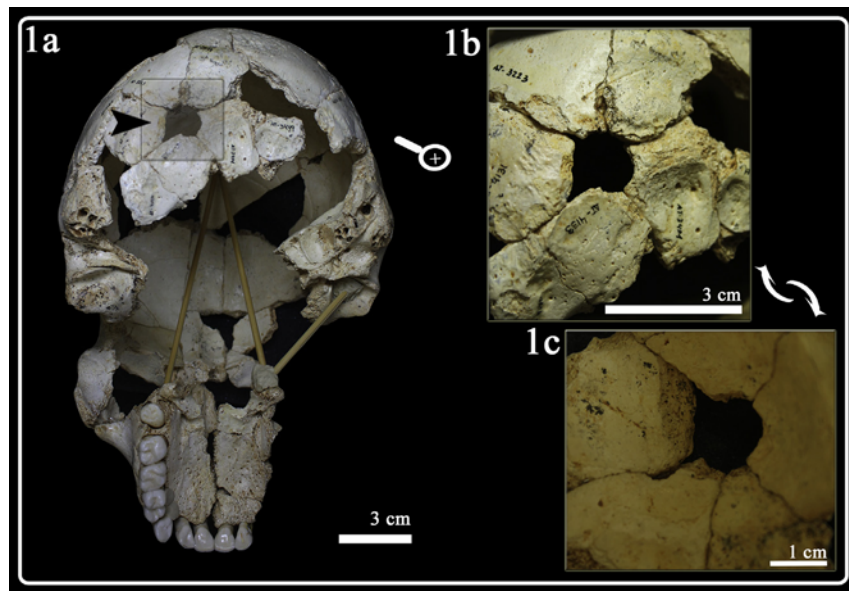


Fig. 8. Cranium 9 (Cr-9) perimortem fracture on the occipital bone. 1a) Inferior view of Cr-9 with the location of the fracture marked with the black arrow; 1b) Detail of the depressed fracture in ectocranial view; 1c) Detail of the depressed fracture in endocranial view.

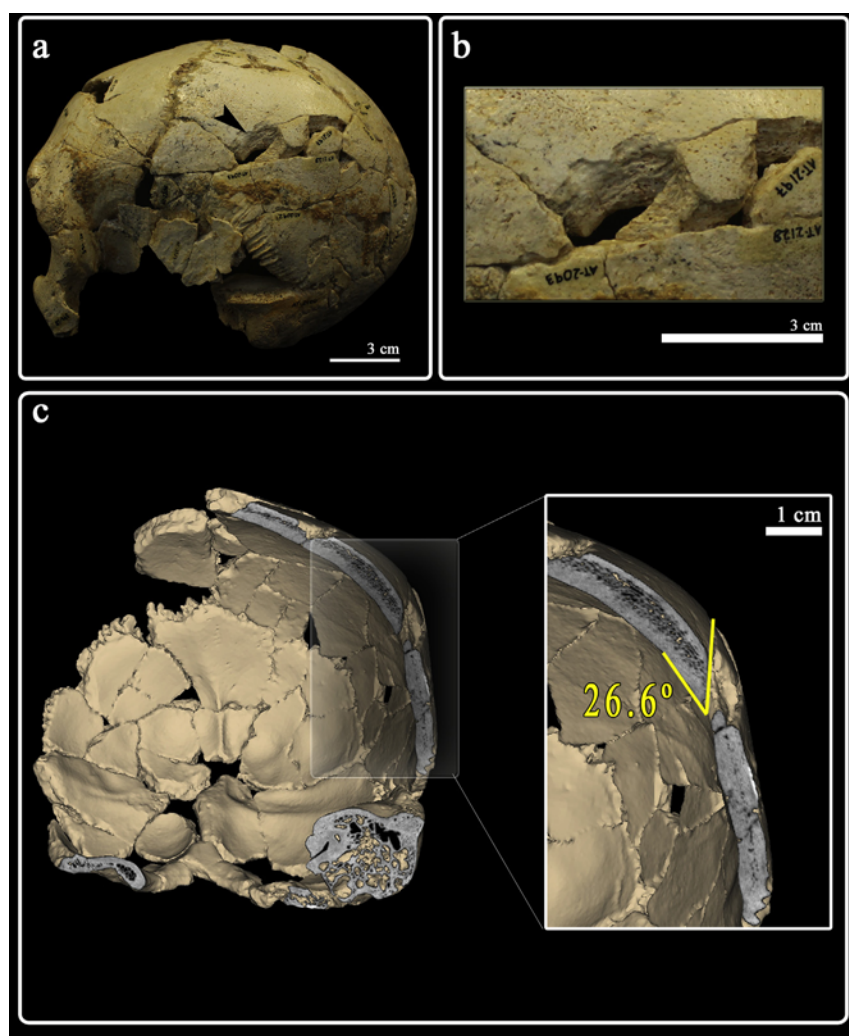


Fig. 9. Cranium 11 (Cr-11) fracture on the left parietal bone. a) Cr-11 in lateral view. The black arrow points to the location of the fracture; b) detailed picture of the fracture in ectocranial view; c) Coronal cross-section at the level of the fracture showing the fracture angle (26.6°).

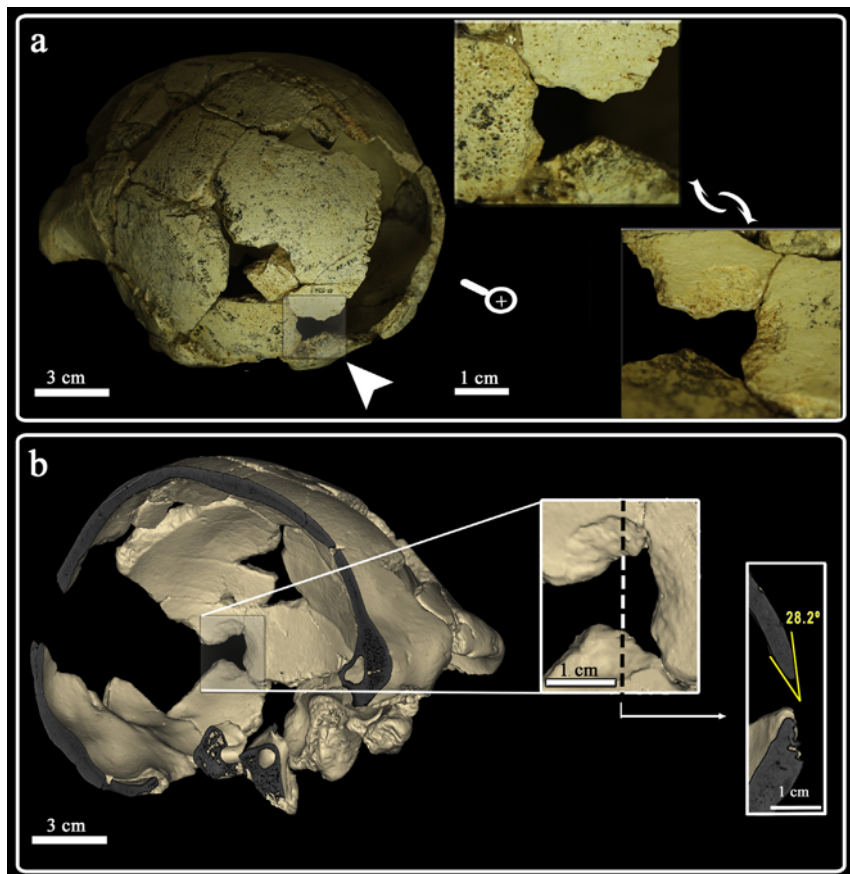


Fig. 10. Cranium 13 (Cr-13) perimortem fracture. a) Cr-13 with the location of the fracture indicated and detailed pictures of the depressed fracture in ectocranial and endocranial views; b) Sagittal cross-section of the Cr-13 virtual CT and detailed pictures showing the cortical delamination in endocranial view and the acute fracture angles (28.2°).

presence of large cortical delamination (Fig. 12).

Therefore, the fracture patterns in the SH cranial sample are dominated (around 96% of the total sample) by straight and curved fractures, right angles, jagged surfaces, fractures interrupted by sutures and the absence of cortical delamination (Table 3). These data have been compared with other archaeological samples. On the one hand, the SH sample has been compared with published assemblages containing fractured fresh bone (Agris and Auzay) and dry bones (Corconne and Villedubert) (Jordana et al., 2013b). Chi square values for SH vs. Agris and SH vs. Auzay show significant differences between the latter assemblages in all features considered ($P < 0.001$). On the other hand, we have compared the fracture patterns with other hominin fossils belonging to Neandertals (La Ferrassie 1, La Chapelle-aux-Saints and La Quina H5) and Upper Paleolithic *H. sapiens* individuals (Cro-Magnon and Abri Pataud) (Table 5) that are considered burials. Fig. 13 shows the fracture pattern of La Ferrassie 1, where postmortem features can be observed.

Chi square values between the SH cranial sample and *Homo* fossils show no significant differences regarding the fracture angle: SH vs. La Ferrassie 1 ($0.88 (P = 0.35)$); SH vs. La Quina H5 ($0.31 (P = 0.57)$); SH vs. A. Pataud ($0.37 (P = 0.53)$) or the presence of cortical delamination: SH vs. La Chapelle-aux-Saints 1 ($0.81 (P = 0.36)$); SH vs. La Ferrassie 1 ($1.26 (P = 0.26)$); SH vs. La Quina H5 ($0.56 (P = 0.21)$); SH vs. Cro-Magnon 1–4 ($1.24 (P = 0.26)$); SH vs. A. Pataud ($0.25 (P = 0.61)$). The only cases in which significant differences are found is when comparing the fracture angles of SH with La Chapelle-aux-Saints 1 (Chi square: $19.72 (P < 0.001)$) and SH vs. Cro-Magnon 1–4 ($4.67 (P = 0.03)$).

4. Discussion

4.1. Timing of the breakage

Taking the features described into account, we can suggest that the general fracture pattern of the SH cranial sample is very similar to those assemblages with dry bone fractures, probably caused by sediment pressure. These data are totally compatible with the data provided by the SH postcranial remains, especially by long bones documenting that, although the majority of the analyzed fractures exhibit postmortem characteristics, a small portion (around 4%) of analyzed long bones display perimortem fractures (Sala et al., 2015a). The same result is obtained by analyzing the SH cranial bones where around 4% of features are different from the postmortem pattern.

Perimortem fractures can be identified by oblique angles, smooth surfaces, the presence of cortical delamination, a pattern of depressed or stellate fracture outlines, and fractures crossing cranial sutures (Table 2). Nevertheless, when any of these features is found isolated in a bone fragment, it is difficult, if not impossible, to determine the timing of bone fracture (Jordana et al., 2013b). Therefore, for caution's sake, we here consider only those individuals who have several perimortem cranial characteristics associated with each other which is the case for Cr-3, Cr-5, Cr-7, Cr-9, Cr-11, Cr-13, Cr-14, and Cr-17 cranial individuals.

Multiple Correspondence Analysis – MCA (Fig. 14) – showed a separation between the fracture properties that depend on the state of the bone when it was fractured (postmortem and perimortem features). Axis 1 (eigenvalue = 0.46843 (10.41% of the

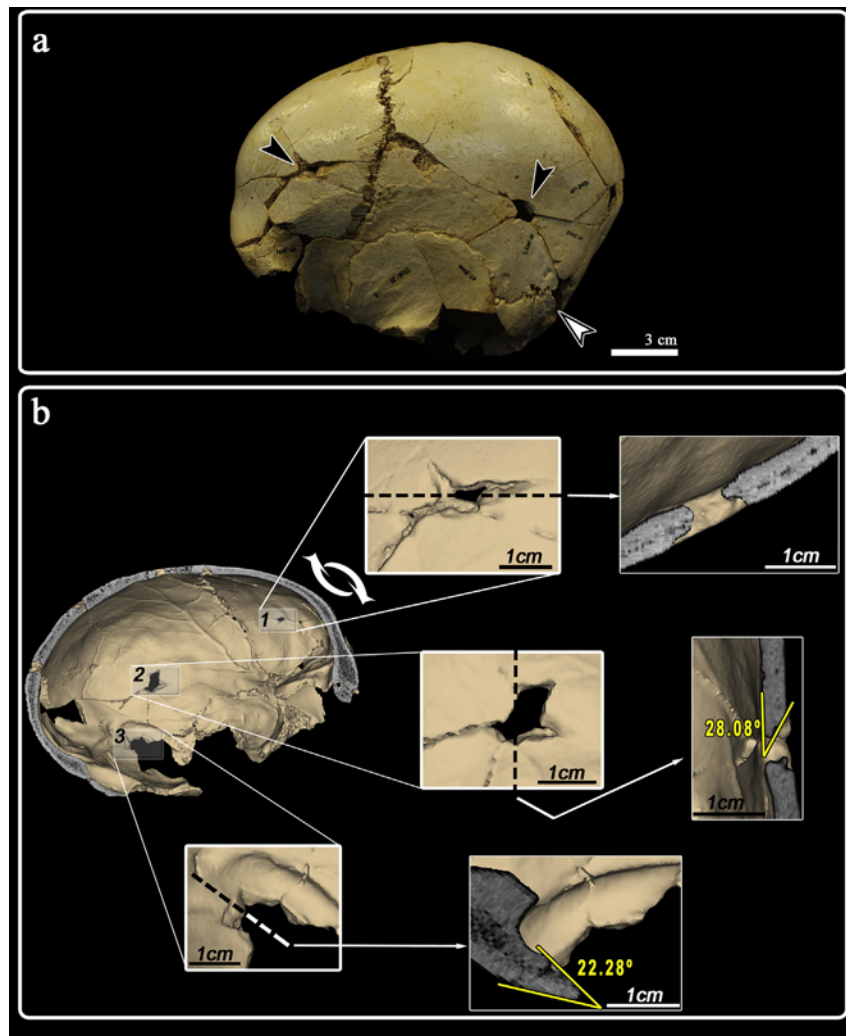


Fig. 11. Cranium 14 (Cr-14) perimortem fractures. a) Cr-14 in lateral view with the location of the fractures indicated; b) CT analysis of the Cranium 14 fractures with a sagittal cross-section where the three fractures are observable in endocranial view on the frontal (1), parietal (2) and occipital (3) bones.

inertia)) clearly distinguishes two sets according to the fracture traits: oblique angles, smooth surfaces, the presence of cortical delamination, the presence of depressed fractures and fractures crossing sutures (typical perimortem traits) versus linear outlines, right angles, an absence of cortical delamination, jagged surfaces and fractures interrupted by sutures (postmortem traits). The SH individuals are distributed regarding these characteristics between those specimens which display only postmortem traits (Cr-1, Cr-2, Cr-6, Cr-8, Cr-10, Cr-15, and Cr-16) and those individuals which, in addition to the postmortem fractures, also display perimortem traits (Cr-3, Cr-5, Cr-7, Cr-9, Cr-11, Cr-13, Cr-14, and Cr-17 cranial individuals).

Regarding other Pleistocene fossils, two specimens affiliate with this last group (mixed features): La Chapelle-aux-Saints and Cro-Magnon 2. These characteristics suggest that these two individuals display perimortem fractures in addition to the postmortem breakage. The mechanism of breakage for these specimens should be explored in future works.

4.2. Mechanisms of breakage

Taking the characteristics of the SH deposit into account, cranial fresh bone fractures could be the result of different possible

scenarios. The first possibility could be perimortem cranial trauma caused during violent actions. Nevertheless, because soft tissue decomposition occurs sometime after the death of the individuals, it is also possible that the perimortem fractures of SH crania could have been produced during the free-fall down the vertical shaft (the mode of entry of the hominin cadavers to the site) accidentally or once the individuals were already dead. Another possibility of perimortem fracturing inside the SH chamber after the body arrived at the site is less likely due to the low energy of the environment during the fossils' deposition (Aranburu et al., 2016; Sala et al., 2015b).

It was previously reported that one cranial individual (Cr-17) displays perimortem traumas caused during a lethal act of interpersonal violence (Sala et al., 2015b). Firstly, the type of injuries (Trauma 1 and Trauma 2) and their location in this specimen are compatible with the forensic criteria to be interpreted as the result of a face-to-face conflict. Furthermore, the dimensions and contours of the two depression fractures were found to be almost indistinguishable (including the presence of a similarly-placed notch in both fracture outlines), strongly suggesting that both fractures were caused by the same object. Lastly, the fractures show different orientations and different trajectories implying that each fracture was caused by an independent impact. If the same object

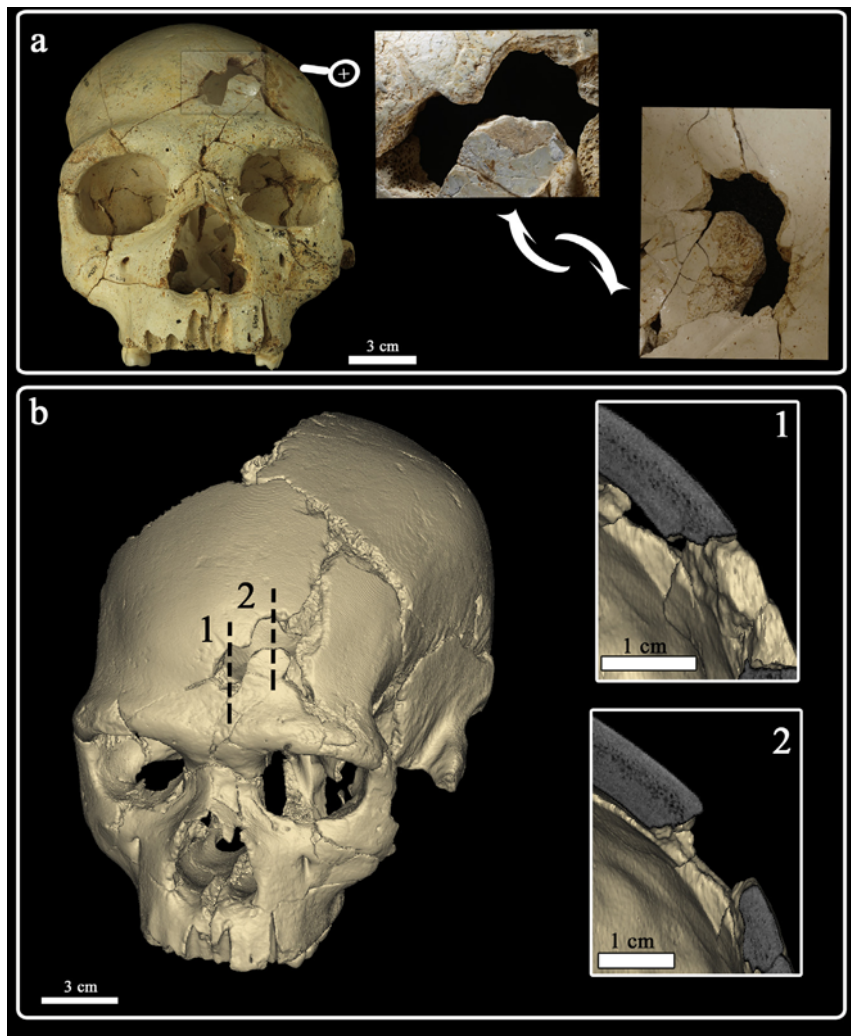


Fig. 12. Cranium 17 (Cr-17) perimortem fractures. a) Frontal view of Cr-17 with detailed perimortem fractures in ectocranial and endocranial views; b) CT analysis of the Cranium 17 traumas and detail of the cross-sections showing the acute angles. Detailed photos by Javier Trueba (Madrid Scientific Films).

Table 5

Fracture properties of the Neandertal and Early *H. sapiens* crania.

Sp.	N	Fracture outline			Angle		Trajectory		Cortical delamination		
		Specimen	N	Linear-straight	Linear-curved	Depressed	Right	Oblique	NCS	CS	Presence
<i>H. n</i>	La Chapelle	16	14 (87.5%)	2 (12.5%)	0	10 (62.5%)	6 (37.5%)	14 (87.5%)	2 (12.5%)	0	16 (100%)
<i>H. n</i>	La Ferrassie-1	25	25 (100%)	0	0	22 (88%)	3 (12%)	25 (100%)	0	0	25 (100%)
<i>H. s</i>	Cro-Magnon-1	1	0	1 (100%)	0	1 (100%)	0	0	1 (100%)	0	1 (100%)
<i>H. s</i>	Cro-Magnon-2	8	6 (75%)	0	2 (25%)	5 (62.5%)	3 (37.5%)	7 (87.5%)	1 (12.5%)	2 (25%)	6 (75%)
<i>H. s</i>	Cro-Magnon-3	4	3 (75%)	1 (25%)	0	4 (100%)	0	3 (75%)	1 (25%)	0	4 (100%)
<i>H. s</i>	Cro-Magnon-4	6	6 (100%)	0	0	6 (100%)	0	6 (100%)	0	0	6 (100%)
<i>H. s</i>	Abri Pataud	5	5 (100%)	0	0	5 (100%)	0	5 (100%)	0	5 (100%)	0
<i>H. n</i>	La Quina H-5	30	29 (96.7%)	1 (3.3%)	0	27 (90%)	3 (10%)	27 (90%)	3 (10%)	0	30 (100%)

Sp: Species: *H. n* (*Homo neanderthalensis*); *H. s* (*Homo sapiens*). N: number of fractures analyzed.

NCS: Not crossing suture. CS: Crossing suture.

likely produced the two independent fractures, any scenario related to the free-fall would require the highly improbable occurrence of the same object striking the skull twice. The same criteria are valid to exclude limestone block-falls inside the SH chamber once the skull was deposited in the site. All these data demonstrate that the Cr-17 blunt force traumas clearly are not accidental, but rather they appear to have been produced by the use of a tool of standardized size and shape and, thus, the most plausible explanation for the

perimortem fractures on Cr-17 is as the result of intentional and repeated blows during a lethal act of interpersonal violence (Sala et al., 2015b).

The next aspect to be analyzed is whether the interpersonal violence was an isolated behavior or if there is more probable evidence for interpersonal violence in the SH population. There is forensic literature dealing with the different criteria to distinguish falls and blows caused in violent events (Guyomarc'h et al., 2010;

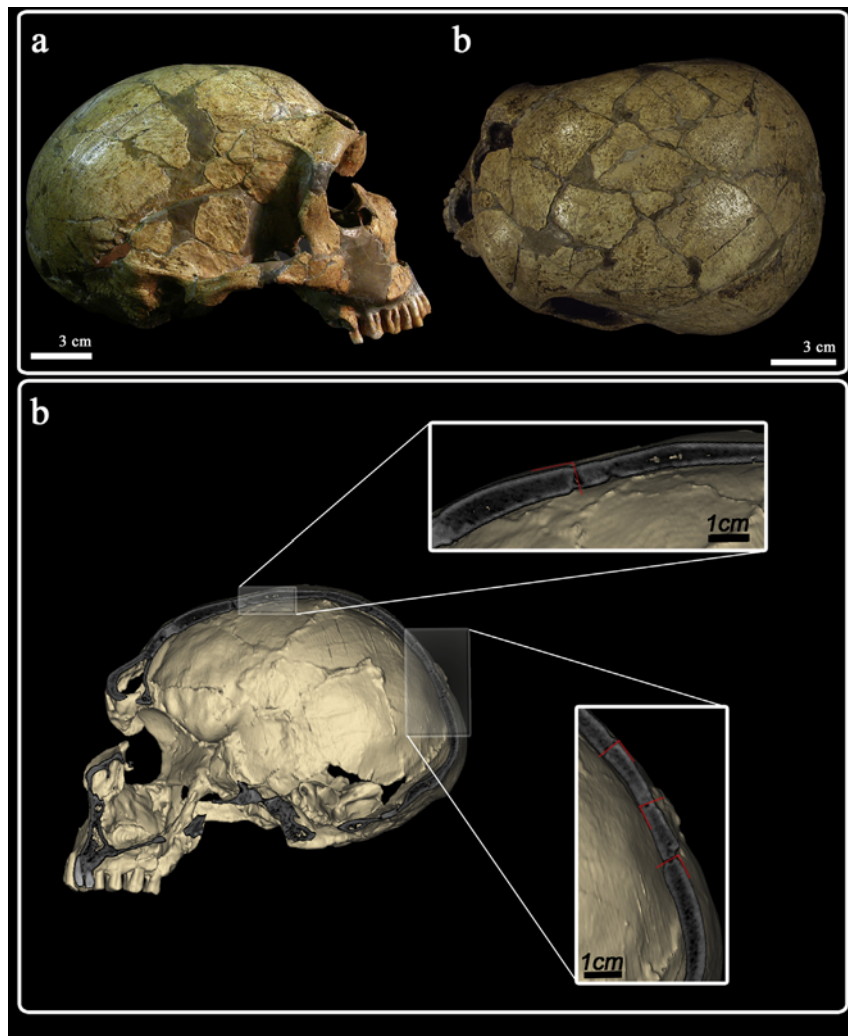


Fig. 13. La Ferrassie 1 Cranium. a) lateral and superior views of the cranium; b) CT analysis of La Ferrassie 1 fractures with a sagittal cross-section showing the typical post-mortem features with right angles (in red) at the breakages points. (For interpretation of the references to color in this figure legend, the reader is referred to the web version of this article.)

Kremer et al., 2008; Kremer and Sauvageau, 2009). Cranial depressed fractures can be a consequence of accidents, although they are more likely to be the result of interpersonal violence (Guyomarc'h et al., 2010; Walker, 1989). Nevertheless, cranial injuries from recent human interpersonal altercations are primarily facial (Galloway, 1999), mostly occur above the "hat brim line", usually show several lacerations, and are predominant on the left side of the vault (Guyomarc'h et al., 2010; Kremer et al., 2008; Kremer and Sauvageau, 2009). Furthermore, other studies use the comparative analysis of size and shape of the fractures as criteria for distinguishing accidental vs. intentional cranial injuries (Sala et al., 2015b; Walker, 1989). We use this multi-criteria approach here in our study of the SH assemblage (Table 6).

In addition to the individual Cr-17, seven more crania (Cr-3, Cr-5, Cr-7, Cr-9, Cr-11, Cr-13, and Cr-14) display evidence of depressed perimortem fractures. None of these cases show evidence of healing (bone remodeling) associated with perimortem fractures. The fractures of the parietal bone observable in Cranium 5 (Cr-5) and Cranium 11 (Cr-11) display the fracture type (depressed fractures) and a position (left side and above the HBL, see Fig. 15) that fit with the criteria that indicate intentional blows.

Cranium 3 (Cr-3) shows two penetrating depressed fractures that are connected on the left side of the occipital squama (within

the HBL zone). This is the expected pattern for localized perimortem blunt force trauma with penetration of the endocranial bone table (Lovell, 1997; Ortner, 2008). The type of injuries, the left side position, and the fact that there are multiple wounds are all compatible with interpersonal violence in this specimen, although the location (posterior plane and within the HBL) is not absolutely conclusive to corroborate this hypothesis. Nevertheless, together with Cr-3, as well as Cr-7, Cr-9, Cr-13, and Cr-14, our data show multiple penetrating depressed fractures of similar size in the posterior region of the crania, in relation to the nuchal plane (Fig. 15). Usually, cranial trauma, from falls or head impacts on blunt objects, tends to produce large comminuted or linear fractures and/or compression of the cranial base (Galloway and Wedel, 2014; Lovell, 1997; Wu et al., 2011). A base fracture is considered to represent a severe injury, since the bone in the cranial base is heavily buttressed (Lovell, 1997). There are three principal types of fractures recognized in the base of the skull that are particularly common in falls from heights: i) Longitudinal, when the fracture divides the base of the crania in right and left halves; ii) Transverse, when the fracture divides the base of the skull into a front and rear half, and iii) Ring fractures, which separate the rim of the foramen magnum from the remainder of the base (Spitz and Spitz, 2006). Instead of these kinds of fractures, Cr-3, Cr-7, Cr-9, Cr-13, and Cr-14

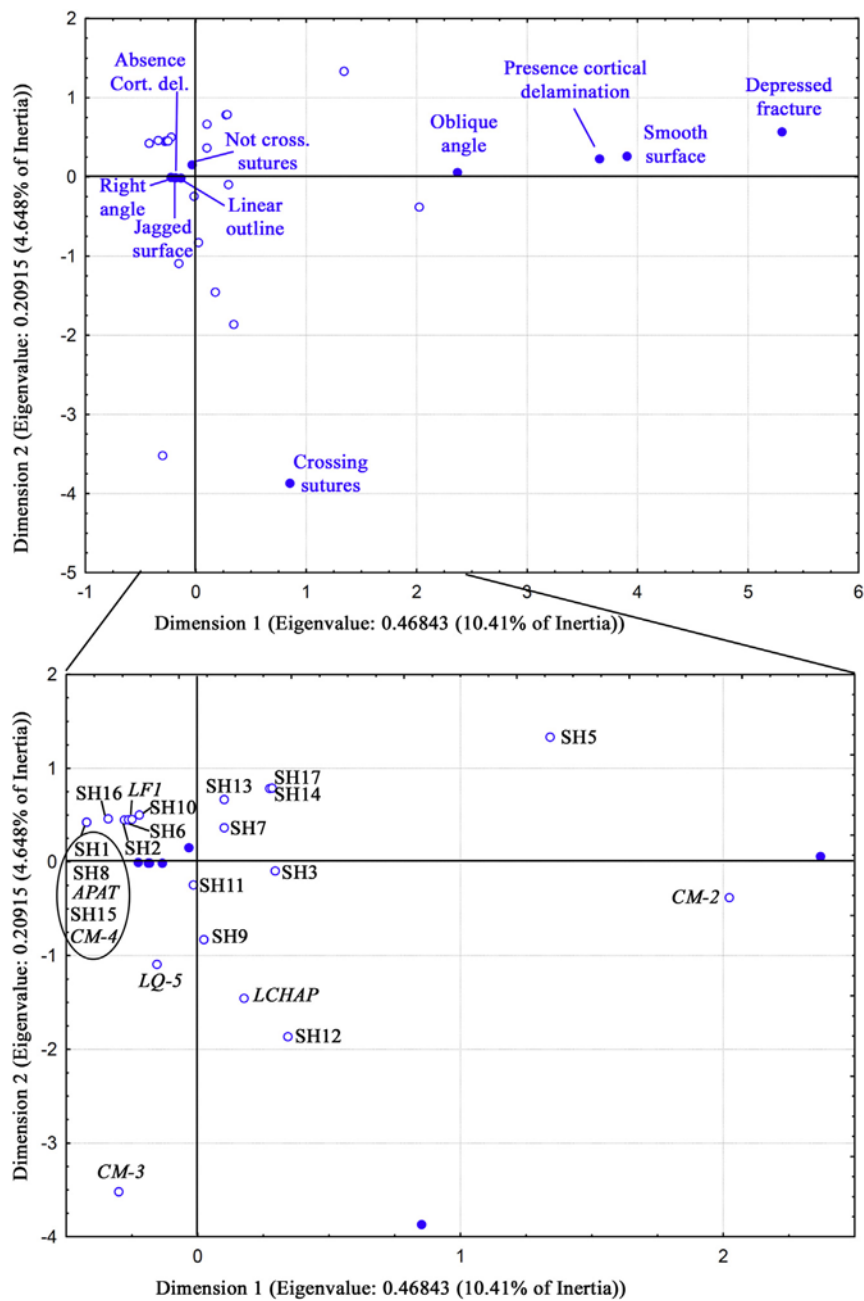


Fig. 14. Multiple Correspondence Analysis (MCA) showing the properties of the fractures (upper image) and the distribution of the fossil samples (lower image) from the present study. Blue circles represent the breakage properties and open circles represent the fossil specimen as follows: SH: Sima de los Huesos (the number is the cranial individual, for example, SH17 = Sima de los Huesos Cr-17); CM: Cro-Magnon; LCHAP: La Chapelle-aux-Saints; LQ5: La Quina 5; LF1: La Ferrassie 1; APAT: Abri Pataud. (For interpretation of the references to color in this figure legend, the reader is referred to the web version of this article.)

Table 6

Fracture type and location of the perimortem fractures of SH crania.

Fracture type	Number fractures	Bone affected	Side	Location with respect to the HBL	
CR-3	Depressed	2	Occipital	Left	Within the HBL
CR-5	Depressed	1	Parietal	Left	Above the HBL
CR-7	Depressed	1	Occipital	Left	Below the HBL
CR-9	Depressed	1	Occipital	Left	Below the HBL
CR-11	Depressed	1	Parietal	Left	Above the HBL
CR-13	Depressed	1	Parietal	Left	Within the HBL
CR-14	Stellate	3	Frontal, parietal and occipital	Left	Above and within the HBL
CR-17	Depressed	2	Frontal	Left	Above the HBL

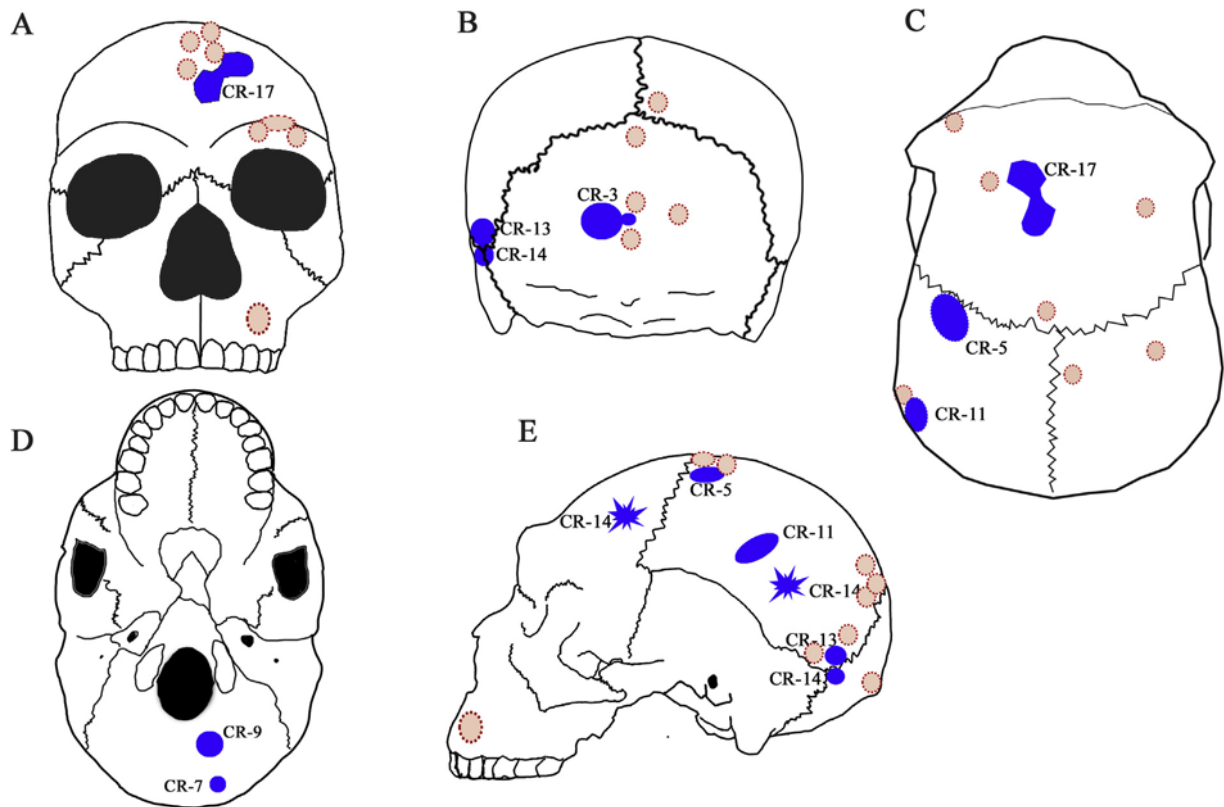


Fig. 15. Location of the perimortem fractures (blue) on Cr-3, Cr-5, Cr-7, Cr-9, Cr-11, Cr-13, Cr-14 and Cr-17 and the healed fractures (red) documented by Pérez et al. (1997) and Gracia-Téllez et al. (2013). A) Anterior; B) Posterior; C) Superior; D) Inferior and E) Lateral views. Circular and oval shapes represent depressed fractures and stars represent stellate fractures. (For interpretation of the references to color in this figure legend, the reader is referred to the web version of this article.)

display penetrating depressed fractures. Penetrating fractures may result from both low and high velocity projectiles (Thomas, 1984). So, the presence of localized penetrating fractures and their nuchal location in these specimens is not what would be expected for accidental falls. Furthermore, the frequency of these kinds of penetrating fractures (five specimens of eight crania with perimortem fractures) with a similar shape in the same region, suggest intentional causes rather than accidental or fortuitous circumstances.

In sum, in the SH cranial sample there is one case which we can interpret with certainty as caused by interpersonal violence: Cr-17. Also Cr-5 and Cr-11 display features absolutely compatible with intentional blows. For the rest of the individuals analyzed, the perimortem fractures could be caused by two agents: a free fall down the vertical shaft that gives access to the SH chamber (either live or already dead individuals), or intentional blows caused by repetitive or recurrent acts of violence. Although the first hypothesis cannot be absolutely rejected, the similarity of the cranial traumas and their location suggest intentional causes as the most plausible hypothesis. This scenario is compatible with the high recurrence of healed depressed cranial injuries (*Supplementary Information Table 2* and Fig. 15) documented previously in the SH sample (Pérez et al., 1997), as well as with the evidence provided by Cr-17.

In addition to the SH cranial sample, the Pleistocene fossil record, contains other evidence of cranial and postcranial perimortem fractures, although there are only few examples that are tentatively considered cases of interpersonal violence: The Shanidar 3 Neandertal shows a penetrating lesion to the left ninth rib (Churchill et al., 2009; Trinkaus, 1983). But, since some bone remodeling is apparent, it is not clear whether the final cause of

death was related to the rib injury. The St. Césaire 1 individual also displays a cranial injury interpreted as inflicted during an act of intragroup interpersonal violence (Zollkofer et al., 2002). The Upper Paleolithic *H. sapiens* individual, Sunghir 1, shows a perimortem sharp trauma in the first thoracic vertebra that has been interpreted as the likely cause of death (Trinkaus and Buzhilova, 2012). The fact that there are only isolated cases of violence documented in the fossil record makes it difficult to interpret whether this behavior was habitual or rare during the Pleistocene. If we accept the interpretation of violence-related causes for the perimortem fractures in the SH cranial sample, we could infer that interpersonal violence occasionally occurred in this Middle Pleistocene population.

5. Conclusions

The application of both taphonomic and forensic criteria, including blunt force trauma analysis, is crucial to approaching the study of Pleistocene hominin fossils and to understanding the site's formation processes. The Sima de los Huesos site has provided a large cranial collection and offers an unprecedented opportunity to perform a complete forensic taphonomic study of a population from the Middle Pleistocene. The results of the present study show that the main fracturation occurred during the dry bone stage and are obviously postmortem fractures. Using a comparative study, the fracture properties are similar to those described in the bibliography for intentional burials of archaeological collections, as well as to the study of fracture patterns in *Homo* specimens (Neandertals and Late Paleolithic *Homo sapiens*) interpreted as intentional burials. Nevertheless, a small portion (around 4% of the fractures analyzed) display the features considered to be results of

perimortem traumas and are present in Cr-3, Cr-5, Cr-7, Cr-9, Cr-11, Cr-13, Cr-14, and Cr-17. This proportion is similar to those found in the postcranial remains studied previously, but cranial remains provide more accurate criteria than postcranial remains for investigating the possible causes of the fracturing. In order to investigate the possible causes for these perimortem traumas, we used forensic criteria. The results show that interpersonal violence is confirmed for one of the skulls, Cr-17 and also probable for Cr-5 and Cr-11. For the rest of the crania, although we cannot rule out that the perimortem fractures could be caused by the free fall down the vertical shaft that gives access to the SH chamber (neither for live or already dead individuals), the similarity of the traumatic fractures and their similar location makes the violence-related scenario the most plausible. This could imply that violent behavior was not an isolated conduct in this Middle Pleistocene population.

Acknowledgements

This study would not have been possible without the work and dedication of the Sima de los Huesos team. For more than 30 years the team have recovered isolated and small cranial fragments that have been carefully reconstructed to form this exceptional collection, especially thanks to Ana Gracia-Téllez. CT scanning was carried out in collaboration with our colleagues of the Laboratorio de la Evolución Humana at the UBU (Spain). We would like to express our gratitude to Dominique Grimaud (MNHN, Paris) for the access to the original specimens of Neandertal and early *Homo sapiens* for comparative purposes with SH and to Aurélie Fort for technical assistance during the stay in Paris. Thanks also to the MNHN curators for providing CT data of fossil specimens. Our most sincere gratitude to Nicholas Conard and to the University of Tübingen for their support. Thanks to Lauren Ames for the English revision of the manuscript and Asier Gómez-Olivencia and Rolf Quam for their advice. Thanks to Javier Trueba (Madrid Scientific Films). Field work at the Sierra de Atapuerca sites was financed by the Junta de Castilla y León and the Fundación Atapuerca. The research was funded by the MINECO projects CGL2012-38434-C03-01 and CGL2015-65387-C3-2-P (MINECO/FEDER). NS has received financial support from University of Tübingen (Project UNESCO 1347021/3900/3034003301). Thanks also to the Fundación Atapuerca (Predoctoral grant to APP in 2015 and Postdoctoral grant to NS in 2014) and to the Real Academia de Doctores de España (Research award to NS in 2013). We would like to thank also the "Grupo de Bioacústica Evolutiva y Paleoantropología (BEP)" research group. This research received support from the SYNTHESYS Project FR-TAF-5135 <http://www.synthesys.info/> which is financed by European Community Research Infrastructure Action under the FP7 "Capacities" Program.

Appendix A. Supplementary data

Supplementary data related to this article can be found at <http://dx.doi.org/10.1016/j.jas.2016.06.001>.

References

- Aguirre, E., 2000. Sima de los Huesos. Escenarios de la formación del yacimiento, crítica y sesgo demográfico. In: Dobón, L.C., Otero, H.R., Compadre, B.S., Martínez, B.L., Blanco, M.J. (Eds.), Tendencias Actuales de Investigación en la Antropología Física Española. Universidad de León, León, pp. 31–42.
- Andrews, P., Fernández-Jalvo, Y., 1997. Surface modifications of the Sima de los Huesos fossil humans. *J. Hum. Evol.* 33, 191–217.
- Aranburu, A., Arsuaga, J.L., Sala, N., 2016. The stratigraphy of the Sima de los Huesos (Atapuerca, Spain) and implications for the origin of the fossil hominin accumulation. *Quat. Int.* <http://dx.doi.org/10.1016/j.quaint.2015.02.044> (in press).
- Arsuaga, J.L., Carretero, J.M., Gracia, A., Martínez, I., 1990. Taphonomical analysis of the human sample from the Sima de los Huesos Middle Pleistocene site (Atapuerca/Ibeas, Spain). *Hum. Evol.* 5, 505–513.
- Arsuaga, J.L., Martínez, I., Gracia, A., Carretero, J.M., Lorenzo, C., García, N., Ortega, A.I., 1997. Sima de los Huesos (Sierra de Atapuerca, Spain). The site. *J. Hum. Evol.* 33, 109–127.
- Arsuaga, J.L., Gracia, A., Lorenzo, C., Martínez, I., Pérez, P.J., 1999. Resto craneal humano de Galería/Cueva de los Zarpazos (Sierra de Atapuerca, Burgos). In: Carbonell Roura, E., Rosas González, A., Díez Fernández-Lomana, J.C. (Eds.), Atapuerca: ocupaciones humanas y paleoecología del yacimiento de Galería. Junta de Castilla y León, pp. 233–235.
- Arsuaga, J.L., Martínez, I., 2004. Atapuerca y la Evolución Humana. Fundación Caixa Catalunya, Barcelona.
- Arsuaga, J.L., Villaverde, V., Quam, R., Martínez, I., Carretero, J.M., Lorenzo, C., Gracia, A., 2007. New Neanderthal remains from Cova Negra (Valencia, Spain). *J. Hum. Evol.* 52, 31–58.
- Arsuaga, J.L., Martínez, I., Arnald, L.J., Aranburu, A., Gracia, A., Sharp, W.D., Quam, R., Falguères, C., Pantoja, A., Bischoff, J., Poza-Rey, E., Parés, J.M., Carretero, J.M., Demuro, M., Lorenzo, C., Sala, N., Martinón-Torres, M., García, N., Alcázar de Velasco, A., Cuenca-Bescós, G., Gómez-Olivencia, A., Moreno, D., Pablos, A., Shen, C.C., Rodríguez, L., Ortega, A.I., García, R., Bonmatí, A., Bermúdez de Castro, J.M., Carbonell, E., 2014. Neandertal roots: cranial and chronological evidence from Sima de los Huesos. *Science* 344, 1358–1363.
- Arsuaga, J.L., Carretero, J.M., Lorenzo, C., Gómez-Olivencia, A., Pablos, A., Rodríguez, L., García-González, R., Bonmatí, A., Quam, R.M., Pantoja-Pérez, A., Martínez, I., Aranburu, A., Gracia-Téllez, A., Poza-Rey, E., Sala, N., García, N., Alcázar de Velasco, A., Cuenca-Bescós, G., Bermúdez de Castro, J.M., Carbonell, E., 2015. Postcranial morphology of the middle Pleistocene humans from Sima de los Huesos. *Spain. Proc. Natl. Acad. Sci.* 112, 11524–11529.
- Bello, S.M., Parfitt, S.A., Stringer, C.B., 2011. Earliest directly-dated human skull-cups. *PLoS One* 6, e17026.
- Bello, S.M., Saladié, P., Cáceres, I., Rodríguez-Hidalgo, A., Parfitt, S.A., 2015. Upper Palaeolithic ritualistic cannibalism at Gough's Cave (Somerset, UK): the human remains from head to toe. *J. Hum. Evol.* 82, 170–189.
- Berger, T.D., Trinkaus, E., 1995. Patterns of trauma among the Neandertals. *J. Archaeol. Sci.* 22, 841–852.
- Bermúdez de Castro, J.M., Martinón-Torres, M., Lozano, M., Sarmiento, S., Muela, A., 2004. Palaeodemography of the Atapuerca-SH Middle Pleistocene hominid sample. A revision and new approaches to the paleodemography of the European Middle Pleistocene population. *J. Anthropol. Res.* 60, 5–26.
- Berryman, H.E., Haun, S.J., 1996. Applying forensic techniques to interpret cranial fracture patterns in an archaeological specimen. *Int. J. Osteoarchaeol.* 6, 2–9.
- Boaz, N.T., Ciochon, R.L., Xu, Q., Liu, J., 2004. Mapping and taphonomic analysis of the *Homo erectus* loci at Locality 1 Zhoukoudian, China. *J. Hum. Evol.* 46, 519–549.
- Bocquet-Appel, J.P., Arsuaga, J.L., 1999. Age distributions of Hominid samples at Atapuerca (SH) and Krapina could indicate accumulation by Catastrophe. *J. Archaeol. Sci.* 26, 327–338.
- Boulestin, B., 2012. Quelques reflexions à propos des coupes crâniennes préhistoriques. In: Boulestin, B., Henry-Gambier, D. (Eds.), Crânes trophiques, crânes d'ancêtres et autres pratiques autour de la tête; problèmes d'interprétation en archéologie. Actes de la table ronde pluridisciplinaire, musée national de Préhistoire, Les Eyzies-de-Tayac (Dordogne, France). 14–16 octobre 2010. BAR International Series 2415. Archaeopress, Oxford, pp. 35–45.
- Boulestin, B., Coupey, A.-S., 2015. Cannibalism in the Linear Pottery Culture: the Human Remains from Herxheim. Archaeopress Publishing LTD, Oxford.
- Cáceres, I., Lozano, M., Saladié, P., 2007. Evidence for Bronze age cannibalism in El Mirador Cave (Sierra de Atapuerca, Burgos, Spain). *Am. J. Phys. Anthropol.* 133, 899–917.
- Coqueugniot, H., Dutour, O., Arensburg, B., Duday, H., Vandermeersch, B., Tillier, A.-M., 2014. Earliest crano-encephalic trauma from the levantine Middle Palaeolithic: 3D reappraisal of the Qafzeh 11 Skull, consequences of pediatric brain damage on individual life condition and social care. *PLoS One* 9, e102822.
- Churchill, S.E., Franciscus, R.G., McKean-Peraza, H.A., Daniel, J.A., Warren, B.R., 2009. Shanidar 3 Neandertal rib puncture wound and paleolithic weaponry. *J. Hum. Evol.* 57, 163–178.
- Defleur, A., 1993. Les sépultures Moustériennes. CNRS, Paris.
- Defleur, A., White, T., Valensi, P., Slimak, L., Crégut-Bonroure, É., 1999. Neanderthal cannibalism at Moula-Guercy, Ardèche, France. *Science* 286, 128–131.
- Díez, J.C., 1990. Estudio tafo-zooarqueológico del Pleistoceno Medio. Aplicación a la Sima de los Huesos. Sierra de Atapuerca. Burgos, I Jornadas Burgalesas de Historia. Introducción a la Historia de Burgos en la Edad Media. Monografías de Historia Castellano-Leonesa, Burgos, pp. 517–530.
- Dirks, P.H., Berger, L.R., Roberts, E.M., Kramers, J.D., Hawks, J., Randolph-Quinney, P.S., Elliott, M., Musiba, C.M., Churchill, S.E., de Ruiter, D.J., Schmid, P., Backwell, L.R., Belyanin, G.A., Boshoff, P., Hunter, K.L., Feuerriegel, E.M., Gurtov, A., Harrison, J.d.G., Hunter, R., Kruger, A., Morris, H., Makhubela, T.V., Peixotto, B., Tucker, S., 2015. Geological and taphonomic context for the new hominin species *Homo naledi* from the Dinaledi Chamber, South Africa. *eLife* 4.
- Evans, F.G., 1957. Stress and Strain in Bones. Their Relation to Fractures and Osteogenesis. Charles C. Thomas, Springfield, Illinois.
- Fleming-Farrell, D., Michailidis, K., Karantanas, A., Roberts, N., Kranioti, E.F., 2013. Virtual assessment of perimortem and postmortem blunt force cranial trauma. *Forensic Sci. Int.* 229, 162.e1–162.e6.
- Galloway, A., 1999. The biomechanics of fracture production. In: Galloway, A. (Ed.), Broken Bones: Anthropological Analysis of Blunt Force Trauma. Charles C. Thomas, Springfield, IL, pp. 35–62.
- Galloway, A., Wedel, V.L., 2014. Bones of the skull, the dentition and osseous structures of the throat. In: Wedel, V.L., Galloway, A. (Eds.), Broken Bones.

- Anthropological Analysis of Blunt Force Trauma, second ed. Charles C. Thomas, Illinois, pp. 133–160.
- Gardner, J.C., Smith, F.H., 2006. The Paleopathology of the Krapina Neandertals. *Period. Biol.* 108, 471–484.
- Gracia-Téllez, A., Arsuaga, J.L., Martínez, I., Martín-Francés, L., Martinón-Torres, M., Bermúdez de Castro, J.M., Bonmatí, A., Liria, J.E., 2013. Orofacial pathology in *Homo heidelbergensis*: the case of Skull 5 from the Sima de los Huesos site (Atapuerca, Spain). *Quat. Int.* 295, 83–93.
- Gurdjian, E.S., Lissner, H.R., 1945. Deformation of the skull in head injury. A study with the stresscoat technique. *Surg. Gynecol. Obstet.* 81, 679–687.
- Guyomarc'h, P., Campagna-Vaillancourt, M., Kremer, C., Sauvageau, A., 2010. Discrimination of falls and blows in blunt head trauma: a multi-criteria approach. *J. Forensic Sci.* 55, 423–427.
- Henry-Gambier, D., 2002. Les fossiles de Cro-Magnon (Les Eyzies-de-Tayac, Dordogne): nouvelles données sur leur position chronologique et leur attribution culturelle. *Paleo* 14, 201–204.
- Johnson, E., 1985. Current developments in bone technology. In: Schiffer, M.B. (Ed.), *Advances in Archaeological Method and Theory*. Academic Press Inc, New York, pp. 157–235.
- Jordana, F., Colat-Parros, J., Bénézech, M., 2013a. Diagnosis of skull fractures according to postmortem interval: an experimental approach in a porcine model. *J. Forensic Sci.* 58, S156–S162.
- Jordana, F., Colat-Parros, J., Bénézech, M., 2013b. Breakage patterns in human cranial bones. *Romanian. J. Leg. Med.* 21, 287–292.
- Jordana, X., Galtés, I., Turbat, T., Batsukh, D., García, C., Isidro, A., Giscard, P.-H., Malgosa, A., 2009. The warriors of the steppes: osteological evidence of warfare and violence from Pazyryk tumuli in the Mongolian Altai. *J. Archaeol. Sci.* 36, 1319–1327.
- Kanz, F., Grossschmidt, K., 2006. Head injuries of Roman gladiators. *Forensic Sci. Int.* 160, 207–216.
- Kimmerle, E.H., Baraybar, J.P., 2008. *Skeletal Trauma: Identification of Injuries Resulting from Human Rights Abuse and Armed Conflict*. CRC Press, Boca Raton.
- Kremer, C., Racette, S., Dionne, C.-A., Sauvageau, A., 2008. Discrimination of falls and blows in blunt head trauma: systematic study of the Hat Brim Line rule in relation to skull fractures. *J. Forensic Sci.* 53, 716–719.
- Kremer, C., Sauvageau, A., 2009. Discrimination of falls and blows in blunt head trauma: assessment of predictability through combined criteria. *J. Forensic Sci.* 54, 923–926.
- Lovell, N.C., 1997. Trauma analysis in Paleopathology. *Yearb. Phys. Anthropol.* 40, 139–170.
- Martin, D.L., Harrod, R.P., 2015. Bioarchaeological contributions to the study of violence. *Yearb. Phys. Anthropol.* 156, 116–145.
- Maureille, B., Peer, P.V., 1998. Une donnée peu connue sur la sépulture du premier adulte de La Ferrassie (Savignac-de-Miremont, Dordogne)/A little known element concerning the burial of the first adult at La Ferrassie (Savignac-de-Miremont, Dordogne). *Paleo* 10, 291–301.
- Messina, A.D., Carotenuto, G., Miccichè, R., Sineo, L., 2013. Fatal cranial injury in an individual from Messina (Sicily) during the times of the Roman Empire. *J. Forensic Leg. Med.* 20, 1018–1023.
- Mirazón-Lahr, M., Rivera, F., Power, R.K., Mounier, A., Copsey, B., Crivellaro, F., Edung, J.E., Fernandez, J.M.M., Kiarie, C., Lawrence, J., Leakey, A., Mbua, E., Miller, H., Muigai, A., Mukhongo, D.M., Van Baalen, A., Wood, R., Schwenninger, J.L., Grün, R., Achyuthan, H., Wilshaw, A., Foley, R.A., 2016. Inter-group violence among early Holocene hunter-gatherers of West Turkana, Kenya. *Nature* 529, 394–398.
- Ortner, D., 2008. Differential diagnosis of skeletal injuries. In: Kimmerle, E.H., Baraybar, J.P. (Eds.), *Skeletal Trauma: Identification of Injuries Resulting from Human Rights Abuse and Armed Conflict*. CRC Press, pp. 21–86.
- Outram, A.K., Knüsel, C.J., Knight, S., Harding, A.F., 2005. Understanding complex fragmented assemblages of human and animal remains: a fully integrated approach. *J. Archaeol. Sci.* 32, 1699–1710.
- Pérez, P.J., Gracia, A., Martínez, I., Arsuaga, J.L., 1997. Paleopathological evidence of the cranial remains from the Sima de los Huesos Middle Pleistocene site (sierra de Atapuerca, Spain). Description and preliminary inferences. *J. Hum. Evol.* 33, 409–421.
- Quatrehomme, G., Iscan, M.Y., 1997. Postmortem skeletal lesions. *Forensic Sci. Int.* 89, 155–165.
- Radovčić, J., Smith, F.H., Trinkaus, E., Wolpoff, M.H., 1988. The Krapina Hominids. An Illustrated Catalog of Skeletal Collection. Croatian Natural History Museum, Mladost, Zagreb.
- Rendu, W., Beauval, C., Crevecoeur, I., Bayle, P., Balzeau, A., Bismuth, T., Bourguignon, L., Delfour, G., Faivre, J.-P., Lacrampe-Cuyaubère, F., Tavormina, C., Todisco, D., Turq, A., Maureille, B., 2014. Evidence supporting an intentional Neandertal burial at La Chapelle-aux-Saints. *Proc. Natl. Acad. Sci.* 111, 81–86.
- Sala, N., Arsuaga, J.L., Martínez, I., Gracia-Téllez, A., 2014. Carnivore activity in the Sima de los Huesos (Atapuerca, Spain) hominin sample. *Quat. Sci. Rev.* 97, 71–83.
- Sala, N., Arsuaga, J.L., Martínez, I., Gracia-Téllez, A., 2015a. Breakage patterns in Sima de los Huesos (Atapuerca, Spain) hominin sample. *J. Archaeol. Sci.* 55, 113–121.
- Sala, N., Arsuaga, J.L., Pantoja-Pérez, A., Pablos, A., Martínez, I., Quam, R.M., Gómez-Olivencia, A., Bermúdez de Castro, J.M., Carbonell, E., 2015b. Lethal interpersonal violence in the Middle Pleistocene. *PLoS One* 10, e0126589.
- Saladié, P., Huguet, R., Díez, C., Rodríguez-Hidalgo, A., Cáceres, I., Vallverdú, J., Rosell, J., Bermúdez de Castro, J.M., Carbonell, E., 2011. Carcass transport decisions in *Homo antecessor* subsistence strategies. *J. Hum. Evol.* 61, 425–446.
- Saladié, P., Huguet, R., Rodríguez-Hidalgo, A., Cáceres, I., Esteban-Nadal, M., Arsuaga, J.L., Bermúdez de Castro, J.M., Carbonell, E., 2012. Intergroup cannibalism in the European Early Pleistocene: the range expansion and imbalance of power hypotheses. *J. Hum. Evol.* 63, 682–695.
- Schultz, M., 2006. Results of the anatomical-paleopathological investigations on the Neanderthal skeleton from Klein Feldhofer Grotte (1856) including the new discoveries from 1997/2000. In: Schmitz, R.W. (Ed.), *Neanderthal 1856–2006*. Verlag Philipp von Zabern, pp. 278–318.
- Sládek, V., Trinkaus, E., Sevcáková, A., Halouzka, R., 2002. Morphological affinities of the Sal'a frontal bone. *J. Hum. Evol.* 43, 787–815.
- Spencer, S.D., 2012. Detecting violence in the archaeological record: clarifying the timing of trauma and manner of death in cases of cranial blunt force trauma among pre-Columbian Amerindians of West-Central Illinois. *Int. J. Paleopathol.* 2, 112–122.
- Spitz, W.U., Spitz, D.J., 2006. In: Spitz and Fisher's Medicolegal Investigation of Death: Guidelines for the Application of Pathology to Crime Investigation, fourth ed. Charles C. Thomas, Springfield.
- Thomas, L.M., 1984. Injury of the head and cervical spine. In: Mathog, R.H. (Ed.), *Maxillofacial Trauma*. Williams & Wilkins, Baltimore, pp. 74–78.
- Trinkaus, E., 1983. The Shanidar Neandertals. Academic Press, New York.
- Trinkaus, E., Svoboda, J.A., 2006. Early Modern Human Evolution in Central Europe. The People of Dolní Věstonice and Pavlov. Oxford University Press, New York.
- Trinkaus, E., Buzhilova, A.P., 2012. The death and burial of Sunghir 1. *Int. J. Osteoarchaeol* 22, 655–666.
- Trinkaus, E., Buzhilova, A.P., Mednikova, M.B., Dobrovolskaya, M.V., 2014. The People of Sunghir: Burials, Bodies, and Behavior in the Earlier Upper Paleolithic. Oxford University Press, New York.
- Ubelaker, D.H., Adams, B.J., 1995. Differentiation of perimortem and postmortem trauma using taphonomic indicators. *J. Forensic Sci.* 40, 509–512.
- Villa, P., Mahieu, E., 1991. Breakage patterns of human long bones. *J. Hum. Evol.* 21, 27–48.
- Walker, P.L., 1989. Cranial injuries as evidence of violence in prehistoric southern Calif. *Am. J. Phys. Anthropol.* 80, 313–323.
- Wheatley, B.P., 2008. Perimortem or postmortem bone fractures? An experimental study of fracture patterns in deer femora. *J. Forensic Sci.* 53, 69–72.
- Wieberg, D.A.M., Wescott, D.J., 2008. Estimating the timing of long bone fractures: correlation between the postmortem interval, bone moisture content, and blunt force trauma fracture characteristics. *J. Forensic Sci.* 53, 1028–1034.
- Wu, J.H., Trinkaus, E., 2015. Neurocranial trauma in the Late Archaic human remains from Xujiaoya, Northern China. *Int. J. Osteoarchaeol* 25, 245–252.
- Wu, X.-J., Schepartz, L.A., Liu, W., Trinkaus, E., 2011. Antemortem trauma and survival in the late Middle Pleistocene human cranium from Maba, South China. *Proc. Natl. Acad. Sci.* 108, 19558–19562.
- Zollinger, C.P.E., Ponce de León, M., Vandermeersch, B., Leveque, F., 2002. Evidence for interpersonal violence in the St. Cesaire Neanderthal. *Proc. Natl. Acad. Sci.* 99, 6444–6448.